THE GEOLOGICAL SOCIETY OF AMERICA®

Provenance of late Paleozoic strata in the Yili Basin: Implications for tectonic evolution of the South Tianshan orogenic belt

Hu Huang[1,2,†], Peter A. Cawood[2,3,†], Shijun Ni[4,†], Mingcai Hou[1,†], Zhiqiang Shi[1], and Xiaolong Hu[1]
[1]*State Key Laboratory of Oil and Gas Reservoir Geology and Exploitation, Institute of Sedimentary Geology, Chengdu University of Technology, Chengdu 610059, China*
[2]*Department of Earth and Environmental Sciences, University of St. Andrews, St. Andrews KY16 9AL, UK*
[3]*School of Earth, Atmosphere & Environment, Monash University, Melbourne, VIC 3800, Australia*
[4]*College of Earth Sciences, Chengdu University of Technology, Chengdu 610059, China*

ABSTRACT

The Yili Basin in NW China preserves a late Paleozoic volcano-sedimentary succession, the provenance of which helps to constrain the tectonic evolution of the South Tianshan orogenic belt. U-Pb ages and trace-element and Hf isotopic compositions of detrital zircons from the Late Devonian to earliest early Carboniferous strata in the Yili Basin suggest that the unit contains detritus mainly derived from basement rocks and contemporaneous arc-related volcanic rocks. The age of the unconformable contact between the Dongtujinhe Formation and underlying arc-related volcanic rocks is constrained to ca. 310 Ma. This age is consistent with published data for tectonic exhumation of high- to ultrahigh-pressure ([U]HP) metamorphic rocks from the northern margin of the South Tianshan orogenic belt. Zircon U-Pb ages from the sedimentary rocks, including clasts in conglomerate, indicate that detritus of the Dongtujinhe Formation was derived from multiple sources related to uplift and erosion of the southern Yili–Central Tianshan block. The presence of abundant eclogite clasts in the conglomerate of the Keguqinshan Formation indicates that (U)HP metamorphic rocks in the South Tianshan orogenic belt were exposed and supplied detritus to the southern Yili Basin at ca. 300 Ma. The early Middle Permian clastic rocks are characterized by Early Permian detrital zircons with a single peak at 278 Ma, derived from the postcollision magmatic rocks. During the Late Permian, input of detritus from old volcanic-sedimentary rocks and basement progressively increased. Integration of the provenance data from late Paleozoic strata in the Yili Basin with the time-equivalent northern Tarim and South Tianshan regions provides a record of the northward subduction of the South Tianshan oceanic crust beneath the Yili–Central Tianshan block in the Late Devonian to late Carboniferous (380–310 Ma), followed by continent-continent collision and final amalgamation at ca. 310–300 Ma, with postcollisional extension in the Permian.

INTRODUCTION

The Central Asian orogenic belt (also known as the Altaids) is sandwiched between the Siberian and Baltic cratons to the north and the Tarim and North China cratons to the south (Fig. 1A). It is the largest Phanerozoic accretionary orogen on Earth, recording a major pulse of juvenile crustal growth (Wilhem et al., 2012; Xiao et al., 2015). The orogenic belt formed by multiple accretion and collision events driven by the evolution and closure of the paleo–Asian Ocean (Şengör et al., 1993; Cawood et al., 2009; Han et al., 2011; Wilhem et al., 2012; Xiao et al., 2013; Han et al., 2016a). The South Tianshan orogenic belt is the southernmost part of the Central Asian orogenic belt and resulted from the closure of the South Tianshan Ocean, followed by collision between the Tarim craton to the south and the Yili–Central Tianshan block to the north (Gao et al., 2011; B.F. Han et al., 2011; Y.G. Han et al., 2016a). Final closure of the South Tianshan Ocean has been proposed to mark the termination of the paleo–Asian Ocean in the southwestern corner of the Central Asian orogenic belt (Gao et al., 2009, 2011; Xiao et al., 2009, 2013). However, the proposed timing of the collision between the Tarim craton to the south and the Yili–Central Tianshan block is controversial, varying from Late Devonian to Middle Triassic (Zhang et al., 2007; Xia et al., 2008; Gao et al., 2011; B.F. Han et al., 2011; Y.G. Han et al., 2016a; Wang et al., 2011; Xiao et al., 2013; X.Y. Xu et al., 2013). A late Carboniferous collision has been supported by recent age data from postcollision granites (300–270 Ma; Biske and Seltmann, 2010; Gao et al., 2011; Han et al., 2011) and high- to ultrahigh-pressure ([U]HP) metamorphic rocks (320–310 Ma; Hegner et al., 2010; Su et al., 2010; Klemd et al., 2011; X. Yang et al., 2013) in the South Tianshan orogenic belt. However, some researchers place the major collisional event in the Late Permian to Middle Triassic, based on the ages of two Late Permian radiolarian specimens from ophiolitic mélange (Li et al., 2005) and Triassic zircon U-Pb ages (233–226 Ma) from eclogites (Zhang et al., 2007). Meanwhile, it has also been suggested that the collision along the South Tianshan region terminated in the Late Devonian–early Carboniferous based on a regional unconformity (Xia et al., 2008, 2012; Charvet et al., 2011; X.Y. Xu et al., 2013).

The U-Pb dating of detrital zircons in clastic rocks, combined with Lu-Hf isotope systematics, has been especially effective in evaluating potential source regions for sedimentary rocks, which in turn can be used to constrain models for basin and orogen development, as well as pos-

†Huang—118huanghu@163.com; Cawood—peter.cawood@monash.edu; Ni—nsj@cdut.edu.cn; Hou—houmc@cdut.edu.cn.

GSA Bulletin; May/June 2018; v. 130; no. 5/6; p. 952–974; https://doi.org/10.1130/B31588.1; 14 figures; 1 table; Data Repository item 2017377; published online 20 December 2017.

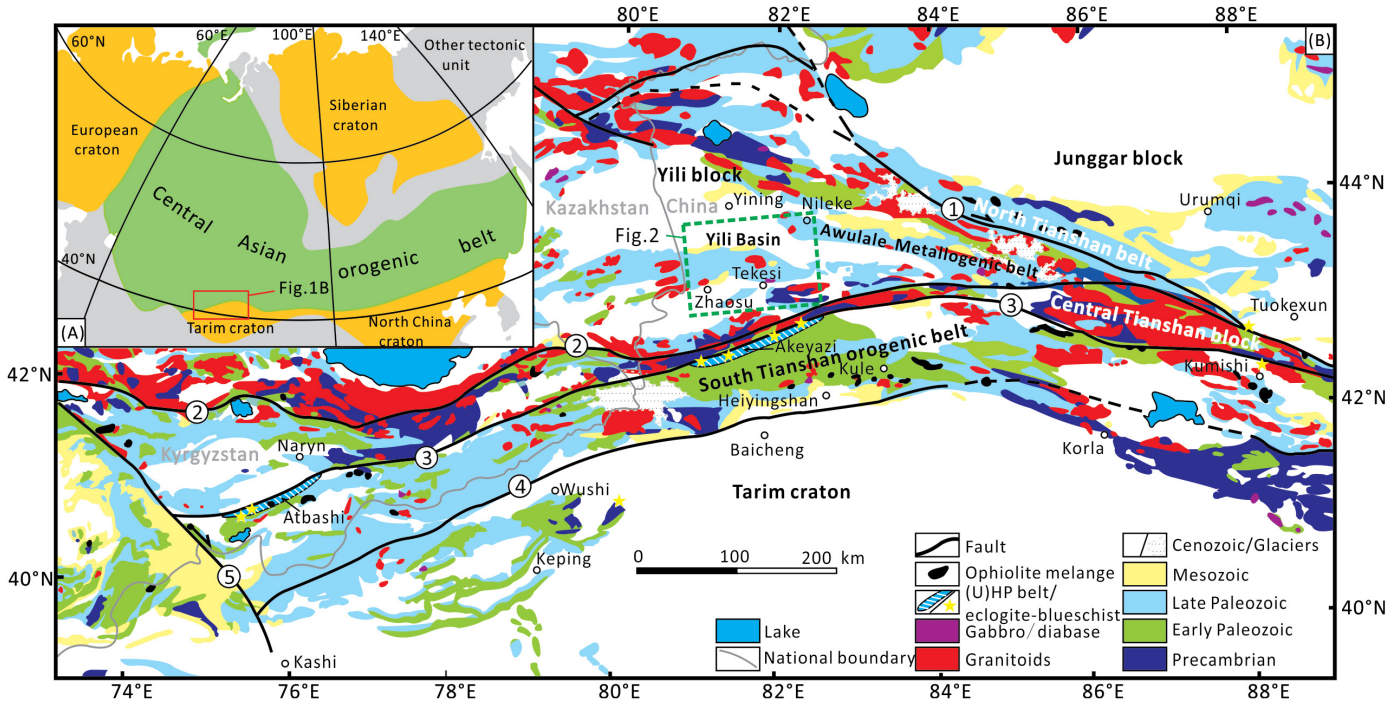

Figure 1. (A) Tectonic sketch map of the Central Asian orogenic belt and adjacent cratonic blocks (modified after Şengör et al., 1993; Windley et al., 2007). (B) Simplified geological map of the western segment of the Tianshan in China-Kyrgyzstan contiguous regions (modified after Gao et al., 2009; Xiao et al., 2013; Han et al., 2016a). 1—North Tianshan fault, 2—Nikolaev Line–North Nalati fault, 3—Atbashi–Inylchek–South Nalati fault, 4—North Tarim fault, and 5—Talas-Ferghana fault. (U)HP—(ultra)high-pressure.

sible feedback mechanisms between these processes (Cawood et al., 2012; Wu et al., 2014). In this paper, we conducted a combined U-Pb and Lu-Hf isotopic study of zircon separates from the late Paleozoic clastic rocks in the Yili Basin, which is situated in the southern Yili–Central Tianshan block, Northwest China. Our results, when combined with data from time-equivalent sequences in the northern Tarim craton (Zou et al., 2013; Y.G. Han et al., 2015, 2016a; Z. Li et al., 2015) and the South Tianshan belt (Carroll et al., 2013; Liu et al., 2013; Han et al., 2016a, 2016b), allow us to better constrain the subduction and collision processes along the South Tianshan orogenic belt and help to resolve existing uncertainties on the timing of collision between the Tarim craton and Yili–Central Tianshan block.

GEOLOGICAL SETTING

The Tianshan orogenic belt forms a collage of lithotectonic blocks situated on the southern margin of the Central Asian orogenic belt. It extends east-west for at least 2500 km from Xinjiang Province in NW China across Kyrgyzstan and southern Kazakhstan to Tajikistan and Uzbekistan (Fig. 1B). The Kyrgyzstan Tianshan is generally divided into the North, Middle, and South Tianshan, and the Chinese Tianshan includes the North Tianshan and South Tianshan blocks and the intervening Yili–Central Tianshan block (Fig. 1B; Gao et al., 2009; Han et al., 2011; Ren et al., 2011). The North Tianshan in Kyrgyzstan and Kazakhstan connects to the Yili block (Gao et al., 2009; Han et al., 2016a). The Chinese Central and South Tianshan are thought to be the eastward continuations of Kyrgyzstan Middle and South Tianshan, respectively, based on similarities in the stratigraphic, magmatic, and detrital zircon records (Gao et al., 2009; Qian et al., 2009; Ma et al., 2012; Kröner et al., 2013; Han et al., 2016a). The Chinese Tianshan is traditionally divided into eastern and western segments roughly along longitude 88°E (Han et al., 2011). This study is mainly focused on the western part of the Tianshan orogenic collage, since the eastern Tianshan has probably undergone a discrete Paleozoic evolution (Y.G. Han et al., 2015, 2016a; Zhang et al., 2016).

The North Tianshan in China is marked by an accretionary complex extending over 300 km between the Junggar block in the north and the Yili block in the south (Fig. 1B). It is bounded by the WNW-striking North Tianshan fault in the south and a N-directed thrust in the north that juxtaposes the accretionary complex over Permian to Cretaceous strata (Han et al., 2010). The accretionary complex belt is mainly composed of Devonian–Carboniferous volcanosedimentary rocks and ophiolitic remnants of the North Tianshan oceanic crust (Han et al., 2010; C. Li et al., 2015). Late Devonian conodonts and early Carboniferous radiolarians have been reported from the siliceous rocks in the accretionary complex, while plagiogranite and gabbro from the Bayingou ophiolite yielded zircon U-Pb ages of ca. 343–325 Ma (Xu et al., 2006; C. Li et al., 2015), consistent with a model in which the North Tianshan belt was formed by subduction of North Tianshan oceanic crust.

The triangular-shaped Yili block is sandwiched between the Junggar block and Central Tianshan block, and it widens westward into Kazakhstan and Kyrgyzstan (Fig. 1B). This tectonic domain is underlain by Mesoproterozoic to Neoproterozoic basement rocks, including granitic gneiss, amphibolite, migmatite, quartzite, marble, and various schists (Li et al., 2009; B. Wang et al., 2014a, 2014b). Mesoproterozoic to Neoproterozoic carbonates and clastic rocks of the Qingbaikou, Jixian, and Changcheng Groups are developed in the Wenquan and Tekesi areas (H.L. Wang et al., 2007). The Precambrian sedimentary-metamorphic rocks are overlain by several Paleozoic volcanosedimentary successions (Xia et al., 2004, 2012;

Zhu et al., 2009). The Awulale metallogenic belt, known for hosting numerous Fe-Cu-Au-Mo deposits (Ge et al., 2015; Z.S. Jiang et al., 2014; N.B. Li et al., 2015a), is located in the transitional zone between the southern Yili block and northern Yili bock (Fig. 1B). It mainly consists of Carboniferous–Permian sedimentary and volcanic rocks, along with minor Mesoproterozoic metamorphic basement rocks, all overlain by Mesozoic and Cenozoic sedimentary rocks (Tang et al., 2010; Ge et al., 2015; N.B. Li et al., 2015a). The Central Tianshan block is separated from the Yili block by the Nikolaev Line–North Nalati fault (Gao et al., 2009; Han et al., 2016a). The Central Tianshan block is characterized by Precambrian basement overlain by Paleozoic volcano-sedimentary rocks, which were intruded by numerous Ordovician–Permian granitoids (Shu et al., 2013; Gou and Zhang, 2016). Although the time of amalgamation between the Yili block and the Central Tianshan block is not well constrained, they were probably united to form the Yili–Central Tianshan block before the Devonian (Gao et al., 2009; Qian et al., 2009; Biske and Seltmann, 2010; X.Y. Xu et al., 2013; Xia et al., 2014). This timing for juxtaposition of the two blocks is based on the presence of Ordovician molasse and adakitic diorites (Qian et al., 2009; Biske and Seltmann, 2010) and Silurian S-type granites (X.Y. Xu et al., 2013).

The South Tianshan orogenic belt is located between the Yili–Central Tianshan block to the north and the Tarim craton to the south, and it is bounded by the Atbashy–Inylchek–South Nalati fault in the north and the North Tarim fault in the south (B.F. Han et al., 2011; Y.G. Han et al., 2016a). The belt is composed mainly of Late Ordovician to late Carboniferous marine volcano-sedimentary rocks and Permian continental clastic and volcanic rocks, followed by Triassic–Jurassic continental clastic rocks (Liu et al., 2013; Xiao et al., 2013; B.F. Han et al., 2011; Y.G. Han et al., 2016a). The Atbashi and Akeyazi (U)HP metamorphic belt occurs along the Atbashy–Inylchek–South Nalati fault, and many ophiolitic mélanges are scattered throughout the South Tianshan orogenic belt (Fig. 1B; Han et al., 2011; Klemd et al., 2011). The ophiolitic mélanges formed in the Late Silurian to early Carboniferous, as evidenced by well-constrained zircon U-Pb ages of 430–330 Ma (Wang et al., 2011; Jian et al., 2013; T. Jiang et al., 2014) and Early Devonian to early Carboniferous radiolarians (Wu and Li, 2013).

The Tarim craton is characterized by a double-layer structure consisting of Precambrian crystalline basement, composed of an Archean tonalitic-trondhjemitic-granodioritic (TTG) suite, orthogneisses, amphibolites, and schists, and a Neoproterozoic cover series (Z.Q. Xu et al., 2013; Zhao et al., 2015). These are in turn overlain by Cambrian and Ordovician strata, which are composed mainly of thick carbonate successions, unconformably covered by Silurian to Devonian clastic rocks (Y.G. Han et al., 2015; Z. Li et al., 2015; He et al., 2016). Carboniferous strata consist of marine clastic and carbonate rocks (Han et al., 2016a). Early–Middle Permian strata are characterized by marine clastic rocks intercalated with carbonates and volcanic rocks, which pass upwards to Late Permian terrestrial sedimentary rocks (Zou et al., 2013; Han et al., 2016a; He et al., 2016).

STRATIGRAPHY AND SAMPLING

In order to understand the tectonic evolution of the South Tianshan orogenic belt, this study is focused on the late Paleozoic strata in the southern part of the Yili Basin. Samples from the Late Devonian to Carboniferous units were collected from the Tekesi and Zhaosu areas in the southern Yili Basin (Fig. 2). Restricted exposures of Permian strata occur in the southern Yili Basin, but they are widely exposed in the Awulale metallogenic belt. We collected samples from the Permian strata in the Zhaosu and Nileke areas for the provenance analysis (Fig. 2).

Dahalajunshan Formation

The Upper Devonian–Lower Carboniferous Dahalajunshan Formation in the southern part of the Tekesi area consists of conglomerates, sandstones, mudstones, gray limestones, and volcanic rocks, totaling ~4300 m in thickness (Fig. 3). The conglomerates unconformably overlie limestones of the Kushitai Group, are clast-supported, and are composed of pebble- to cobble-sized clasts that are poorly sorted (Fig. 4A). The upward-fining sandstone-mudstone packages (commonly 1.5–2.0 m thick) are separated from one another by abrupt erosion surfaces along their bases, and they commonly exhibit normal grading. The conglomerates, sandstones, and mudstones in the lower part of the Dahalajunshan Formation were deposited in a fan-delta environment (Bai et al., 2015a, 2015b). The gray limestones are commonly 10–20 cm thick and formed in a shallow-marine environment (Bai et al., 2015b). The upper 2900 m section of the Dahalajunshan Formation is mainly composed of rhyolites, andesites, and basaltic andesites.

Akeshake Formation

The Akeshake Formation consists mainly of bioclastic limestones, pebbly sandstones, and cross-bedded, coarse-grained sandstones. The lower part of the Akeshake Formation is dominated by pebbly sandstones, tuffaceous sandstones, and coarse-grained sandstones and contains plant fossils. The sandstone beds exhibit abundant low-angle planar cross-bedding and high-angle trough cross-stratification. The paleocurrent data from the cross-stratification reveal a northwestward paleoflow direction (Fig. 3). The limestones contain abundant fossil assemblages, including coral, foraminifera, crinoid stems, and brachiopod shells. The Akeshake Formation is interpreted to have accumulated in a braided-delta environment passing up to a shallow-marine carbonate unit (Fig. 3; Xiong et al., 2011).

Dongtujinhe Formation

The Dongtujinhe Formation in the southern Yili Basin is only exposed in the Tekesi area and displays an unconformable contact with the underlying volcanic rocks of the Upper Carboniferous Yishijilike Formation (Figs. 3 and 4B). The lower 150 m section of the Dongtujinhe Formation consists mainly of sandstones, pebbly sandstones, and thick-bedded conglomerates. Conglomerates are clast supported, poorly sorted, subangular, and of pebble to cobble grade, ranging from 5 mm to 30 cm, with most in the range 5–10 cm. Desiccation cracks and plant debris are common in the purple-red pebbly sandstones and sandstones (Fig. 4C). Fossils, including foraminifera, corals, and bivalve and brachiopod shells, are observed in the upper part of the formation. The depositional environment of the Dongtujinhe Formation in the Tekesi area changed from a debris flow–dominated fan-delta environment to a shallow-marine environment (Fig. 3; Zhang et al., 2006).

Keguqinshan Formation

The Keguqinshan Formation, which is sporadically exposed in the southern Yili Basin, unconformably overlies the Dongtujinhe Formation and other older strata (Y.J. Li et al., 2011). In the southern part of the Tekesi area, the Keguqinshan Formation unconformably overlies limestones of the Kushitai Group. The formation is ~100 m thick and mainly consists of gray thick-bedded conglomerates and minor wedges and lenses of pebbly sandstone interbeds (~20–70 cm in thickness). The conglomerates are clast supported and composed of pebble- to cobble-sized clasts that are poorly sorted and subangular to subrounded. Clast imbrication was not observed. The lithofacies association is interpreted as indicating deposition in an alluvial-fan setting (Blair and McPherson, 1994). The paleocurrent data from the cross-stratification

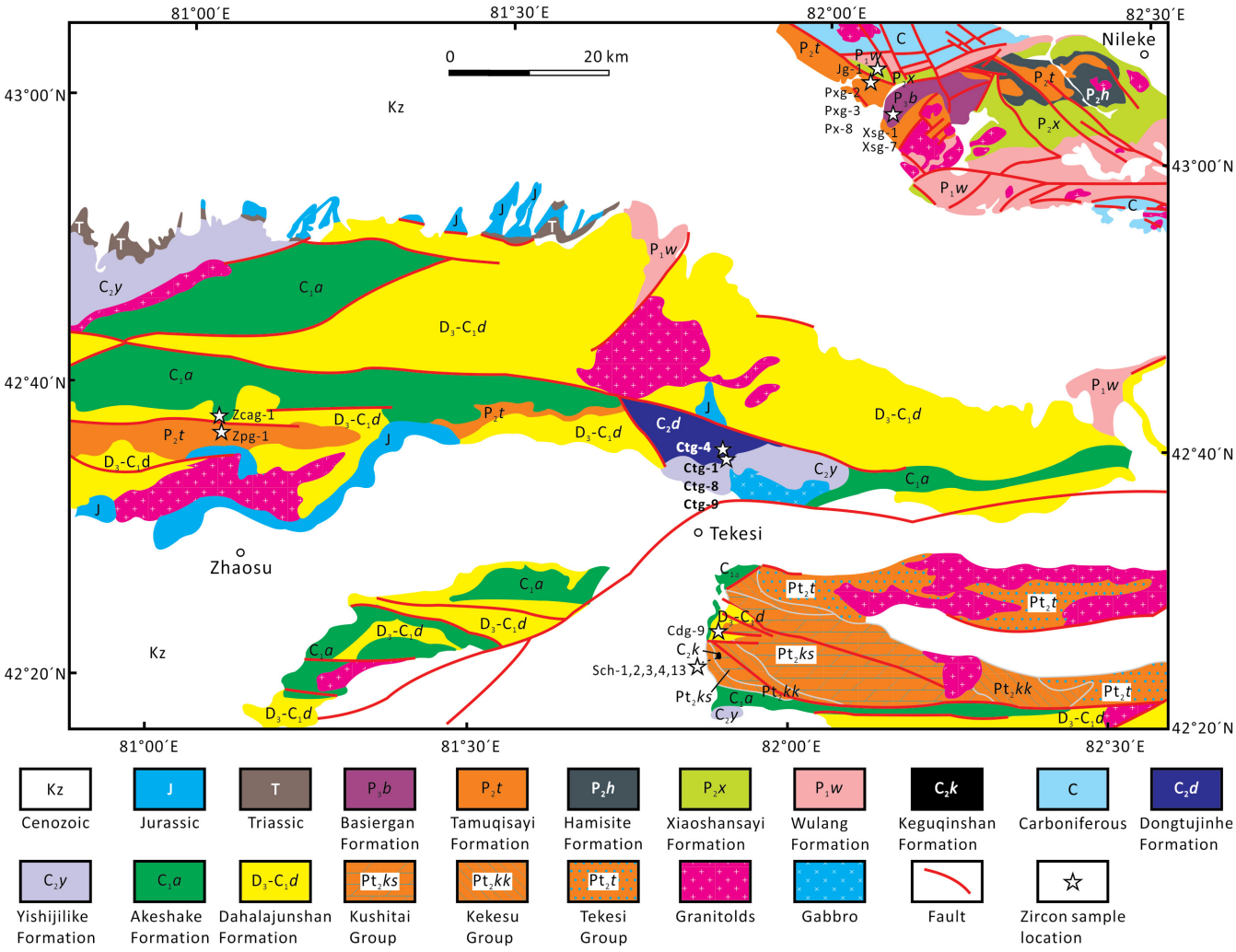

Figure 2. Geological map of the Zhaosu-Tekesi-Nileke area showing the sampling locations (modified after Zhang et al., 2006; B. Wang et al., 2007; N.B. Li et al., 2015a). Abbreviations: Pt_2—Mesoproterozoic; D_3-C_1—Late Devonian–early Carboniferous; C_1—early Carboniferous; C_2—late Carboniferous; P_1—Early Permian; P_2—Middle Permian; P_3—Late Permian.

(Fig. 4D) reveal a northwestward paleoflow direction (Fig. 3).

Xiaoshansayi Formation

The Xiaoshansayi Formation conformably overlies the volcanic rocks of the Lower Permian Wulang Formation. The formation is ~800 m thick and mainly composed of purple-red and gray thick-bedded conglomerates, pebbly sandstones, sandstones, siltstones, and mudstones (Song et al., 2005; N.B. Li et al., 2015a; W.L. Ma et al., 2015). Conglomerates are clast supported and subangular to subrounded, and they display erosive basal contacts. The average clast size is ~5 cm in the long dimension, with a maximum clast size of ~20 cm. Upward-fining trends, cross-bedding, and trough cross-stratification are observed in individual sandstone beds. The sandstone cross-sets indicate an approximately N-directed paleocurrent (Fig. 3). Three depositional environments characterize the clastic deposits of the Xiaoshansayi Formation: fan-delta, braided-river, and shallow-lacustrine systems (Fig. 3; W.L. Ma et al., 2015).

Tamuqisayi Formation

The Tamuqisayi Formation conformably overlies the volcanic rocks of the Middle Permian Hamuqisayi Formation at Nileke and unconformably underlies the Akeshake Formation at Zhaosu. It mainly consists of red and gray thick-bedded conglomerates, sandstones, siltstones, and mudstones. Conglomerates are both clast and matrix supported, subangular, and of pebble to cobble grade, ranging from 5 mm to 80 cm at Nileke (Fig. 4F) and 5 mm to 20 cm at Zhaosu. Imbricated conglomerates with paleocurrent directions at Zhaosu suggest sediment transport from south to north (Fig. 3). The sandstone beds are separated by erosion surfaces. Desiccation cracks and plant debris are common in the sandstones. The clastic rocks of the Tamuqisayi Formation were deposited in alluvial-fan, braided-river, and deep-lacustrine environments (Fig. 3; Song et al., 2005; W.L. Ma et al., 2015).

Basiergan Formation

The Basiergan Formation in the Yili Basin is only exposed in the Nileke area, where it

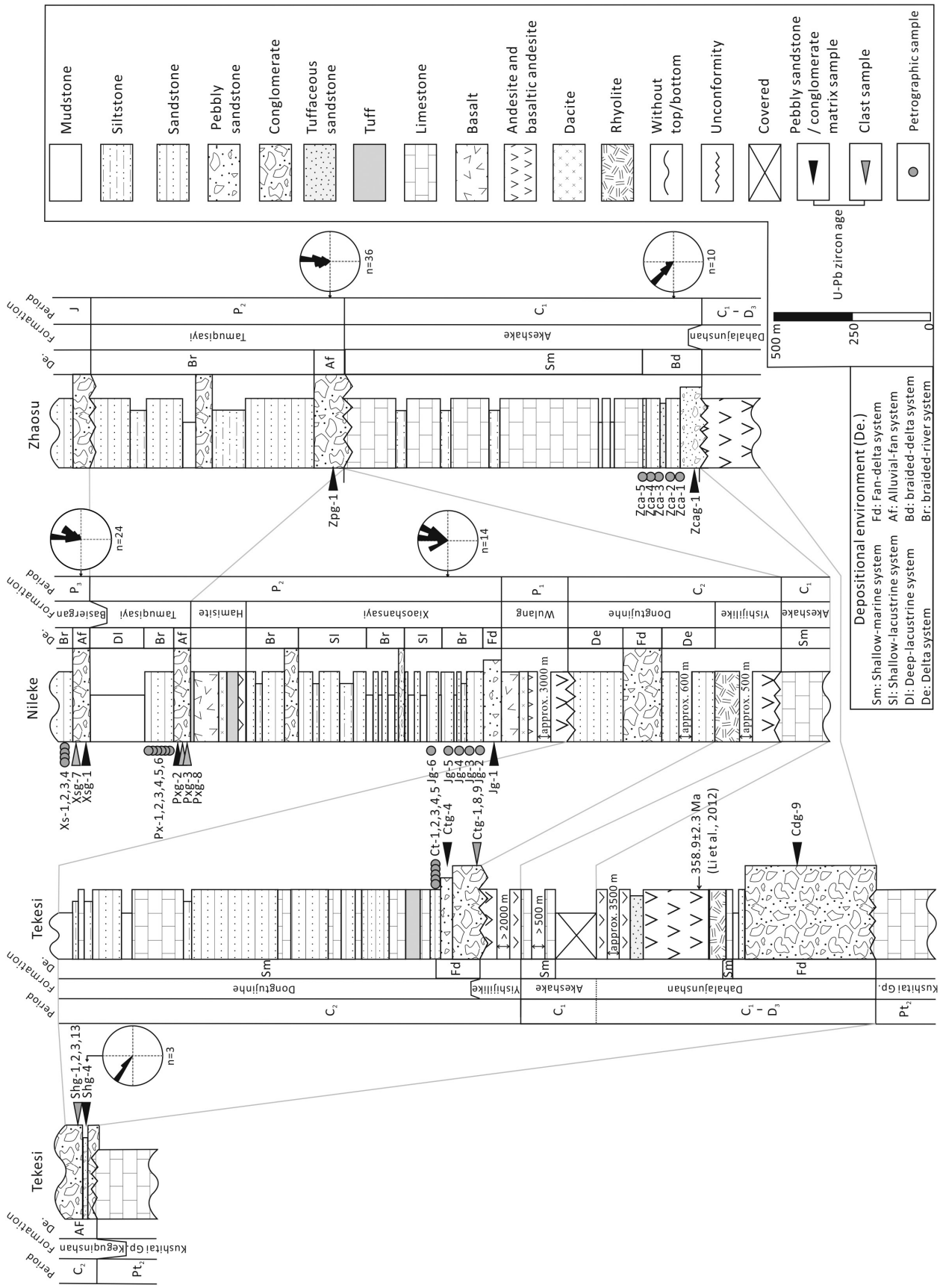

Figure 3. Simplified stratigraphic columns and depositional environments for the late Paleozoic strata at Tekesi, Nileke, and Zhaosu (modified after Song et al., 2005; Zhang et al., 2006; Wang et al., 2009; Xiong et al., 2011; Li et al., 2012; D. Li et al., 2015; W.L. Ma et al., 2015), showing stratigraphic position of analyzed samples. Abbreviations: Pt_2—Mesoproterozoic; D_3-C_1—Late Devonian–early Carboniferous; C_1—early Carboniferous; C_2—late Carboniferous; P_1—Early Permian; P_2—Middle Permian; P_3—Late Permian; J—Jurassic.

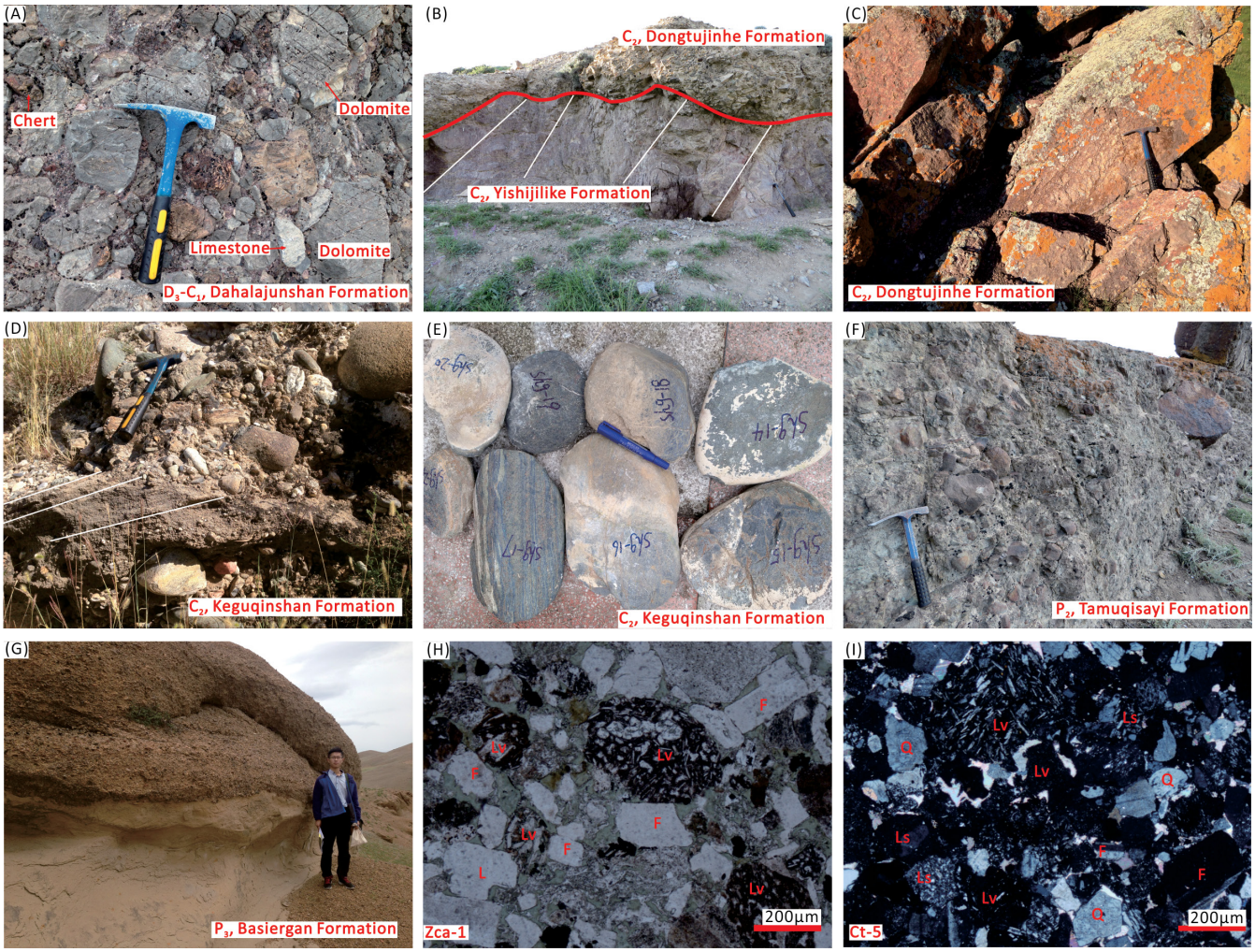

Figure 4. Representative field photographs and photomicrographs of the late Paleozoic succession in the Yili Basin: (A) Conglomerate of the Dahalajunshan Formation at Tekesi; (B) unconformable contact between the Dongtujinhe Formation and the Yishijilike Formation at Tekesi; (C) purple-red pebbly sandstones of the Dongtujinhe Formation at Tekesi; (D) cross-beds in pebbly sandstones of the Keguqinshan Formation at Tekesi; (E) eclogite clasts in the conglomerate of the Keguqinshan Formation at Tekesi; (F) conglomerates of the Tamuqisayi Formation at Nileke; (G) conglomerates of the Basiergan Formation at Nileke displaying erosive basal contacts; (H) sandstone sample from the Akeshake Formation at Zhaosu (sample Zca-1) and (I) sandstone sample from the Dongtujinhe Formation at Tekesi (sample Ct-5). H and I are in plane-polarized light and cross-polarized light, respectively. Q—quartz, F—feldspar, Ls—sedimentary lithic, Lv—volcanic lithic. D_3-C_1—Late Devonian–early Carboniferous; C_2—late Carboniferous; P_2—Middle Permian; P_3—Late Permian.

conformably overlies the Tamuqisayi Formation. It mainly consists of red thick-bedded conglomerates and sandstones. Conglomerates are clast supported and subangular to subrounded, and they display erosive basal contacts (Fig. 4G). Upward-fining trends, cross-bedding, and plant debris are common in the sandstone beds. Paleocurrent indicators, including cross-beds and clast imbrication, suggest sediment transport from south to north (Fig. 3). The Basiergan Formation is interpreted to have been deposited in alluvial-fan and braided-river environments (Fig. 3; Song et al., 2005; W.L. Ma et al., 2015).

ANALYTICAL METHODS

Compositional Methods

To determine the provenance of the late Paleozoic rock units in the Yili Basin, conglomerate and sandstone compositional data were collected (Fig. 3). Conglomerate clast counts were conducted throughout the studied stratigraphic sections in 15 localities. Compositional data for 25 standard petrographic sections were point-counted according to the Gazzi-Dickinson method (Ingersoll et al., 1984). Modal analyses of framework components were based on 400–500 grains per thin section, and these are listed in Supplementary Table S1.[1]

Zircon U-Pb Dating and Hf Isotopes

Eighteen samples, including four matrix and ten clast samples from conglomerate beds and

[1]GSA Data Repository item 2017377, supplementary data for representative zircon cathodoluminescence images, sandstone modal composition, zircon U-Pb and Hf analyses, and zircon trace element concentration, is available at http://www.geosociety.org/datarepository/2017 or by request to editing@geosociety.org.

four pebbly sandstone samples, were collected for zircon analysis (Fig. 3). Zircons grains were separated by standard density and magnetic techniques, prior to handpicking under a binocular microscope and mounting in epoxy and polishing for backscattered electron (BSE) and cathodoluminescence (CL) imaging. U-Pb dating and trace-element analyses of zircon were simultaneously conducted by laser ablation–inductively coupled plasma–mass spectrometry (LA-ICP-MS) at the State Key Laboratory of Geological Processes and Mineral Resources (GPMR), China University of Geosciences, Wuhan. Detailed operating conditions for the laser-ablation system and the ICP-MS instrument and data reduction followed the methodology outlined by Liu et al. (2010). Laser sampling was performed using a Geolas 2005, and ion-signal intensities were acquired by an Agilent 7500a ICP-MS instrument. The laser beam had a diameter of 32 μm, a repetition frequency of 6 Hz, and laser energy of ~60 mJ. Ablated zircon materials were transported into the ICP-MS by He, mixed with Ar carrier gas. The signal acquisition time was set to be 50 s, after a 20–30 s blank acquisition interval. Zircon standard 91500 ($^{206}Pb/^{238}U$ age = 1062.4 ± 0.4 Ma; Wiedenbeck et al., 1995) was used as an external standard for U-Pb dating, and it was analyzed twice every six analyses. Off-line selection and integration of background and signals, and time-drift correction and quantitative calibration for trace-element analyses and U-Pb dating were performed by ICPMSDataCal (Liu et al., 2010). Common Pb correction was not performed, because the measured ^{204}Pb signal was low, and the U-Pb ages were concordant or nearly concordant. Concordia diagrams and weighted mean age calculations were conducted using the ISOPLOT program (Ludwig, 2003). Zircon standard GJ-1 was analyzed as an unknown, and the obtained mean $^{206}Pb/^{238}U$ age was 599.6 ± 1.0 Ma (2σ, n = 64, mean square of weighted deviates [MSWD] = 0.33), in good agreement with the recommended age (599.8 ± 1.7 Ma [2σ]; Jackson et al., 2004). The $^{206}Pb/^{238}U$ ages are preferred for zircons with ages younger than 1000 Ma, and $^{207}Pb/^{206}Pb$ ages are preferred for grains older than 1000 Ma. Uncertainties on individual analyses in the data table and on concordia plots are presented at 1σ, whereas errors on averages of multiple analyses are given at the 95% confidence level. Trace-element compositions of zircons were calibrated against reference materials BCR-2G and BIR-1G, combined with internal standardization (Liu et al., 2010). The preferred values of element concentrations for the U.S. Geological Survey (USGS) reference glasses are from the GeoReM database (http://georem.mpch-mainz.gwdg.de/). The average analytical error ranges from ~±10% for light rare earth elements (LREEs) to ~±5% for the other rare earth elements (REEs).

In situ zircon Lu-Hf isotopic analysis was carried out on a Neptune Plus multicollector (MC) ICP-MS (Thermo Fisher Scientific, Bremen, Germany) in combination with a Geolas 2005 excimer ArF laser-ablation system (Lambda Physik, Göttingen, Germany) hosted at the GPMR. Analytical spots were located close to, or on the top of, spots used for U-Pb analysis or in the same growth domain as inferred from CL images. Detailed operating conditions for the laser-ablation system, the MC-ICP-MS instrument, and analytical method are the same as described by Hu et al. (2012). The analyses were conducted with a beam diameter of 44 μm and a repetition rate of 6 Hz. Zircon standards 91500 and GJ-1 were used as the reference standards. Off-line selection and integration analyte signals, and isobaric interference and mass fractionation correction of Lu-Hf isotopic ratios were also performed by ICPMSDataCal (Liu et al., 2010). The obtained Hf isotopic composition was 0.282023 ± 0.000019 (2σ, n = 57) for GJ-1, comparable with the recommended value of 0.282000 ± 0.000005 (Morel et al., 2008). The decay constant adopted for ^{176}Lu was 1.865×10^{-11} yr^{-1} (Scherer et al., 2001). The value of $\varepsilon_{Hf}(t)$ was calculated relative to the chondritic reservoir with a $^{176}Hf/^{177}Hf$ ratio of 0.282772 and $^{176}Lu/^{177}Hf$ ratio of 0.0332 (Blichert-Toft and Albarède, 1997). The single-stage model age (T_{DM1}) was calculated relative to the depleted mantle with a present-day $^{176}Hf/^{177}Hf$ ratio of 0.28325 and $^{176}Lu/^{177}Hf$ ratio of 0.0384 (Griffin et al., 2000), and two-stage model ages (T_{DM2}) were calculated by assuming a mean $^{176}Lu/^{177}Hf$ value of 0.015 for the average continental crust (Vervoort and Blichert-Toft, 1999). Initial $^{176}Hf/^{177}Hf$ ratios and $\varepsilon_{Hf}(t)$ values were calculated using the zircon crystallization ages.

RESULTS

Conglomerate Clast Counts

Clasts of dolomite, limestone, chert, and quartzite dominate the conglomerates in the Dahalajunshan Formation (Fig. 5A) and are inferred to have originated mainly from basement rocks (Xia et al., 2004; Bai et al., 2015a). Clasts in conglomerates from the Akeshake Formation mainly consist of basalts with minor limestones (Fig. 5B). Conglomerates in the Dongtujinhe Formation contain abundant sandstone and volcanic (rhyolite and andesite) clasts, with some limestone, chert, mudstone, quartzite, and reworked conglomerate clasts (Fig. 5C). The composition of conglomerate clasts from the Keguqinshan Formation is granites, quartzites, eclogites (Fig. 4E), limestones, and sandstones (Fig. 5D). Clast counts of the conglomerates in the Permian strata at Nileke display an up-section decrease in the relative abundance of volcanic clasts, accompanied by an increase in quartzite clasts (Figs. 5E–5H). Gray bioclastic limestone clasts compose up to 20% of the total clasts in the Tamuqisayi Formation at Nileke (Fig. 5F). Granite, granitic gneiss, and quartz schist clasts are also observed in the conglomerates of the Xiaoshansayi Formation (Fig. 5H).

Sandstone Modal Compositions

The studied sandstone samples are texturally and mineralogically immature, exhibiting angular to subangular grains with minor alteration, and contain mud infill or calcite cement. Compositionally, sandstones of the Akeshake Formation are mainly composed of lithic and feldspar grains, and they lack quartz (Fig. 6A). The dominant lithic fragments are intermediate to basic volcanic rocks with lathwork and microlitic textures (Fig. 4H). Sandstones of the Dongtujinhe Formation at Tekesi, and the Xiaoshansayi and Tamuqisayi Formations at Nileke have similar Q-F-L (quartz [Q] - feldspar [F] - lithic fragments [L]) modal compositions (Fig. 6A). Among the lithic fragments, sedimentary and volcanic rocks are the major constituents of samples from the Dongtujinhe (Fig. 4I) and Tamuqisayi Formations. Sedimentary lithic fragments are rare in the Xiaoshansayi Formation samples (Fig. 6B). The Basiergan Formation samples are characterized by abundant quartz grains and an abrupt increase in the quantity of metamorphic fragments (Fig. 6).

Zircon U-Pb Ages

All analyses are presented in Supplementary Table S2 (see footnote 1). In total, 883 analyses were undertaken on 881 zircon grains, of which 88 analyses showed greater than 10% discordance and were excluded. The remaining 795 analyses give U-Pb ages ranging from 3181 Ma to 264 Ma. Most Archean to Mesoproterozoic and some Neoproterozoic zircons are subrounded to well rounded, with lengths ranging from 50 to 180 μm and aspect ratios between 1:1 and 3:1 (Supplementary Fig. S1 [see footnote 1]). Compared with Precambrian zircons, most Paleozoic zircons are more euhedral/prismatic and larger in size (80–300 μm in length), with aspect ratios between 1:1 and 4:1 (Supplementary Fig. S1 [see footnote 1]). Most zircon grains show clear, oscillatory zoning in CL images (Supplementary Fig. S1 [see footnote 1]) and

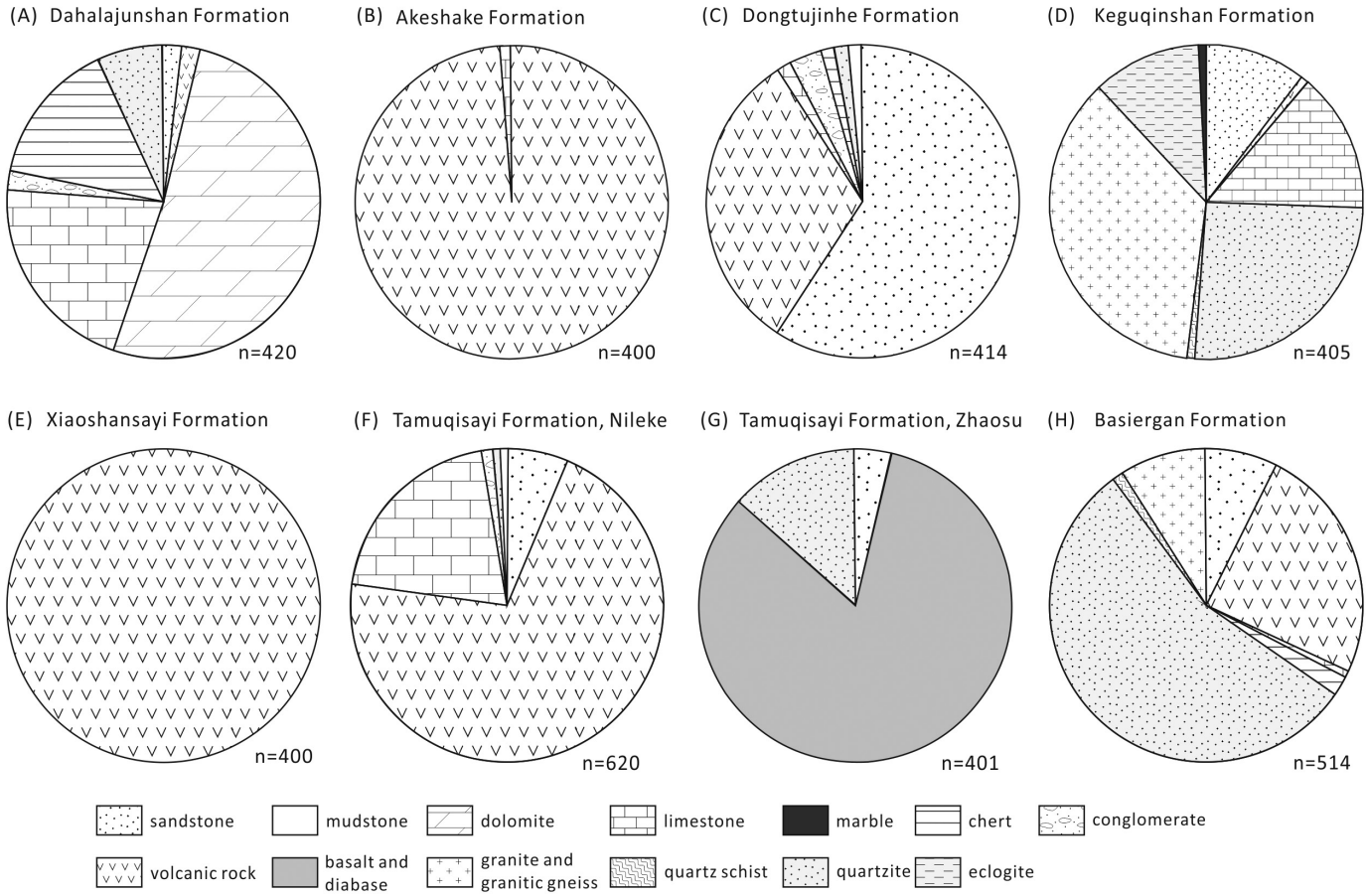

Figure 5. Conglomerate clast compositional data for the late Paleozoic strata in the Yili Basin.

high Th/U ratios (mostly 0.2–2.6), indicative of a magmatic origin. Two grains (Xsg-1–40 and Xsg-1–71) with Mesoproterozoic ages display homogeneous CL structures (Supplementary Fig. S1 [see footnote 1]) and have low Th/U ratios (<0.1), suggesting a possible metamorphic origin.

Dahalajunshan Formation Sample Cdg-9 (D_3-C_1)

Seventy-one analyses on 71 detrital zircon grains were undertaken on conglomerate matrix sample Cdg-9 from the Upper Devonian–Lower Carboniferous Dahalajunshan Formation. Sixty-three analyzed ages displayed concordance greater than 90% and ranged in age from 3180 Ma to 360 Ma. Major age groups occur at 380–360 Ma, 460–430 Ma, and 505–480 Ma, and a subordinate age group occurs at 1800–1050 Ma (Fig. 7A). Other age components are minor and scatter at ca. 415, 575, 950–600, 2250–2000, 2500, and 3180 Ma.

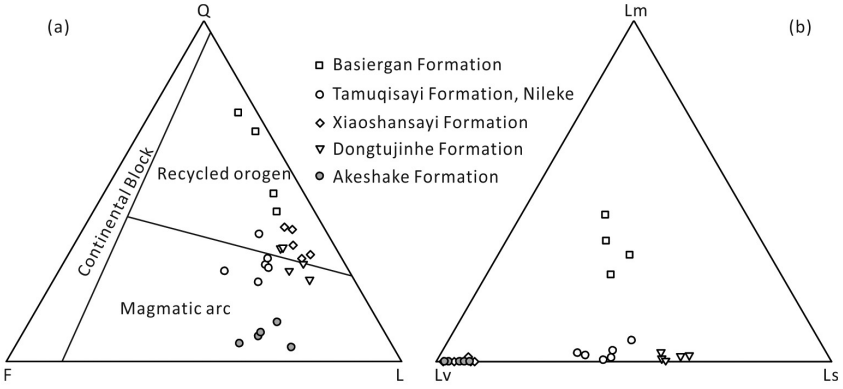

Figure 6. Sandstone petrographic data from the studied samples including Q-F-L (quartz, feldspar, and lithic clasts; Dickinson et al., 1983) and Lm-Lv-Ls (metamorphic, volcanic, and sedimentary lithics) ternary plots.

Akeshake Formation Sample Zcag-1 (C_1)

Sixty-five analyses on 65 detrital zircon grains were undertaken on the pebbly sandstone sample Zcag-1 from the Lower Carboniferous Akeshake Formation and yielded two discordant ages. The remaining 63 ages are mainly grouped between 360 Ma and 320 Ma, with a single main peak at 336 Ma (n = 62; Fig. 7B). One analysis yielded an older age of 432 ± 6 Ma.

Dongtujinhe Formation Samples Ctg-1, Ctg-4, Ctg-8, and Ctg-9 (C_2)

Seventy-five analyses on 75 detrital zircon grains from sandstone clast sample Ctg-1 yielded 58 concordant analyses. The measured ages are between 880 Ma and 310 Ma, with a major age group at 350–310 Ma and subordinate age groups at 365–350 Ma and

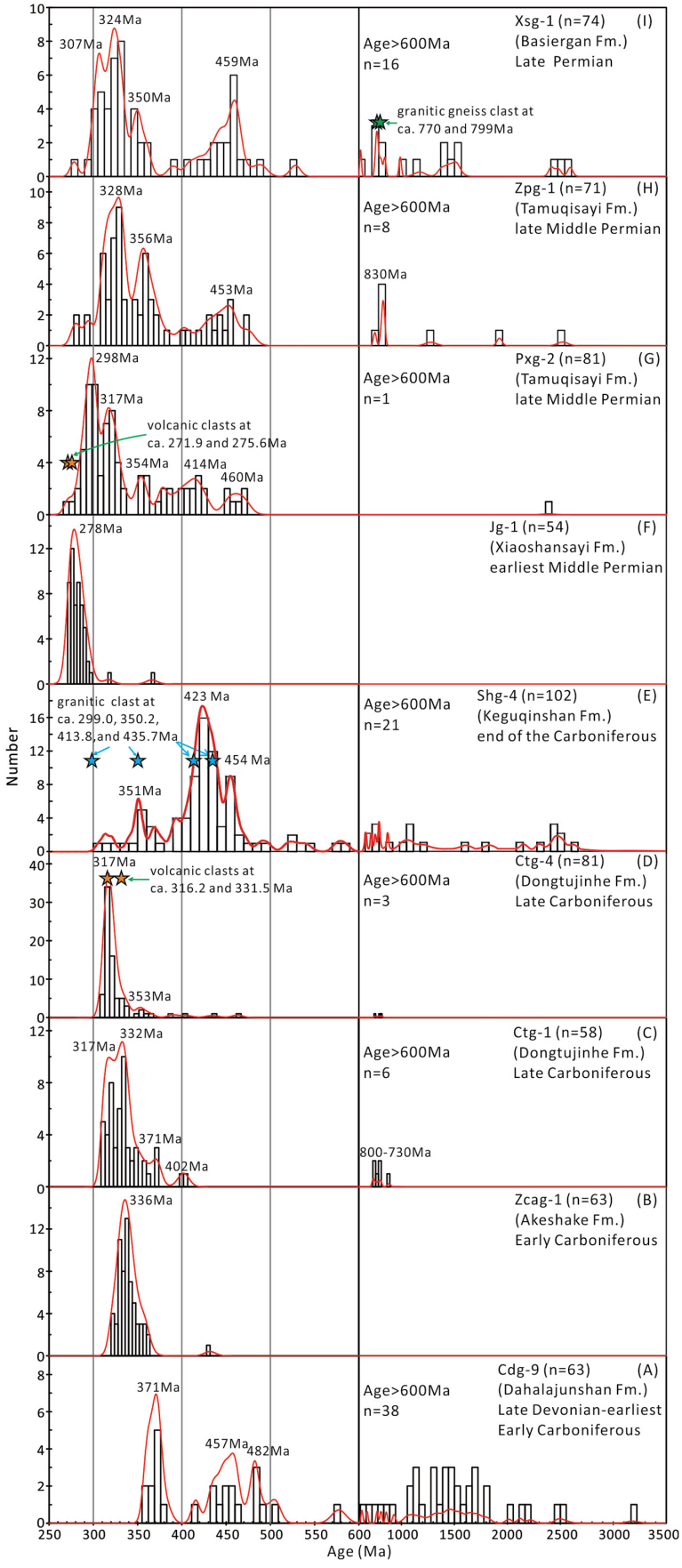

820–760 Ma, with minor scattered ages 460–390 Ma (Fig. 7C).

Of eighty-three analyses on 83 zircons, two were discordant for pebbly sandstone sample Ctg-4. The measured ages range from 820 Ma to 310 Ma, with a major group at 340–310 Ma, and subordinate age groups at 370–360 Ma, 400 Ma, and 880–740 Ma (Fig. 7D).

Twenty-four analyses of 24 zircon grains were undertaken on the rhyolite clast sample Ctg-8, and one analysis was discordant. The remaining 23 concordant ages range from 336 Ma to 328 Ma and give a weighted mean $^{206}Pb/^{238}U$ age of 331.5 ± 2.0 Ma (2σ), with a MSWD value of 0.22 (Fig. 8A).

Fourteen analyses of 14 zircon grains were undertaken on the andesite clast sample Ctg-9. All analyses showed concordant ages, ranging from 320 Ma to 314 Ma, and giving a weighted mean $^{206}Pb/^{238}U$ age of 316.2 ± 2.4 Ma (2σ), with a MSWD value of 0.19 (Fig. 8B).

Keguqinshan Formation Samples Shg-1, Shg-2, Shg-3, Shg-4, and Shg-13 (C_2)

Twenty analyses of 20 zircon grains were undertaken on the granitic clast sample Shg-1. All analyses showed concordant ages, ranging from 412 Ma to 295 Ma. The 15 youngest zircon grains give a weighted mean $^{206}Pb/^{238}U$ age of 299.0 ± 1.7 Ma (2σ), with a MSWD value of 0.51 (Fig. 8C).

Twenty-four analyses of 20 zircon grains were undertaken on the granitic clast sample Shg-2. Eighteen analyses showed concordant ages, ranging from 421 Ma to 409 Ma, and giving a weighted mean $^{206}Pb/^{238}U$ age of 413.8 ± 2.3 Ma (2σ), with a MSWD value of 0.44 (Fig. 8D).

Fifteen analyses of 15 zircon grains were undertaken on the granitic clast sample Shg-3. Fourteen analyses showed concordant ages, ranging from 405 Ma to 340 Ma. The 13 youngest zircon grains give a weighted mean $^{206}Pb/^{238}U$ age of 350.2 ± 2.8 Ma (2σ), with a MSWD value of 0.62 (Fig. 8E).

One hundred and six analyses of 106 detrital zircons grains from the pebbly sandstone sample Shg-4 yielded 102 concordant analyses. The measured ages are between 2611 Ma and 307 Ma, with major age groups at 370–350 Ma

Figure 7. Histograms and probability curves for detrital zircon ages of nine samples from the Yili Basin. The *x*-axis scales are different for portions younger than 600 Ma and older than 600 Ma. The *y* axes for portions younger than 600 Ma are expanded to highlight the Paleozoic zircon populations.

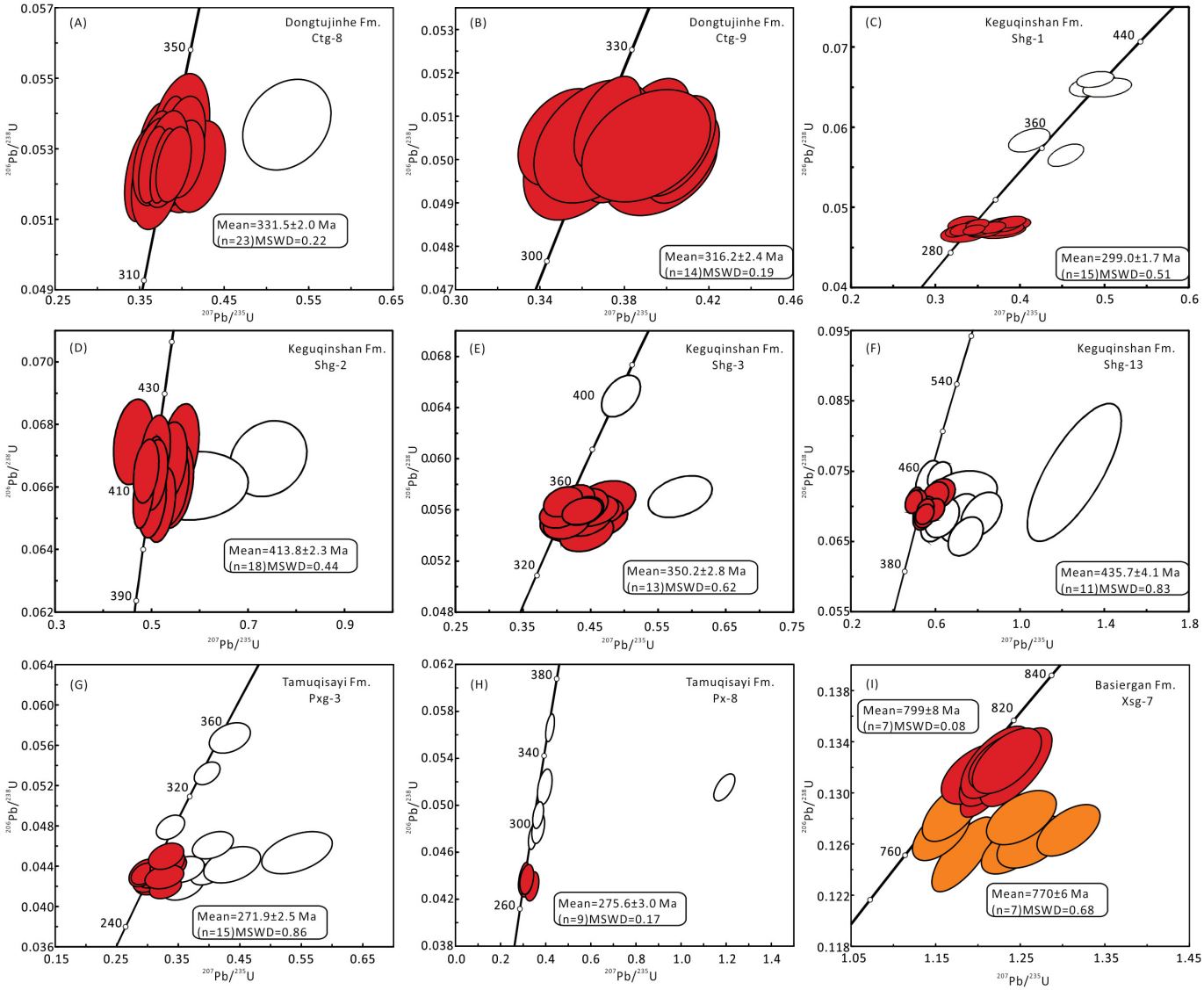

Figure 8. Laser ablation–inductively coupled plasma–mass spectrometry (LA-ICP-MS) zircon U-Pb concordia diagrams for volcanic, granitic, and granitic gneiss clasts from conglomerates of the (A–B) Dongtujinhe and (C–F) Keguqinshan Formations at Tekesi and the (G–H) Tamuqisayi and (I) Basiergan Formations at Nileke. MSWD—mean square of weighted deviates.

and 470–390 Ma, and subordinate age groups at 340–310 Ma, 860–700 Ma, 1200–1000 Ma, and 2600–2300 Ma (Fig. 7E). Other minor ages scatter at ca. 580–490, 650, and 2100–1600 Ma.

Of 20 analyses on 20 zircons grains, 13 were concordant for the granitic clast sample Shg-13. The measured ages are between 462 Ma and 428 Ma. The 11 youngest zircon grains give a weighted mean $^{206}Pb/^{238}U$ age of 435.7 ± 4.1 Ma (2σ), with a MSWD value of 0.83 (Fig. 8F).

Xiaoshansayi Formation Sample Jg-1 (P_2)

Seventy-seven analyses were conducted on 76 detrital zircon grains from the pebbly sandstone sample Jg-1, and these yielded 54 concordant ages. The measured ages mainly range from 365 Ma to 270 Ma, with a single main peak at 278 Ma (n = 52; Fig. 7F). Two analyses yielded older ages of 317 ± 6 Ma and 366 ± 6 Ma.

Tamuqisayi Formation Samples Pxg-1, Pxg-3, Px8, and Zpg-1 (P_2)

Of 84 analyses on 84 detrital zircons grains, 81 were concordant for the conglomerate matrix sample Pxg-1. The measured ages are between 2390 Ma and 270 Ma, with a major age group at 340–270 Ma and subordinate age groups at 360–350 Ma, 390–375 Ma, 430–400 Ma, and 470–450 Ma (Fig. 7G). One analysis yielded an age of ca. 2390 Ma.

Twenty-four analyses of 24 zircon grains were undertaken on the andesite clast sample Pxg-3. Eighteen analyses gave concordant ages, ranging from 355 Ma to 264 Ma. The 15 youngest zircon grains give a weighted mean $^{206}Pb/^{238}U$ age of 271.9 ± 2.5 Ma (2σ), with a MSWD value of 0.86 (Fig. 8G).

Of 15 analyses on 15 zircons grains, 14 were concordant for the dacite clast sample Px-8. The measured ages are between 355 Ma and 272 Ma. The nine youngest zircon grains give a weighted mean $^{206}Pb/^{238}U$ age of 275.6 ± 3.0 Ma (2σ), with a MSWD value of 0.17 (Fig. 8H).

Seventy-seven analyses of 77 detrital zircons grains from the conglomerate matrix sample Zpg-1 yielded 71 concordant analyses. The measured ages are between 2522 Ma and 280 Ma, with major age groups at 340–290 Ma

and 380–350 Ma, and subordinate age groups at 480–430 Ma and 840–750 Ma (Fig. 7H). Other minor ages scatter at ca. 280, 420–400, and 2500–1280 Ma.

Basiergan Formation Sample Xsg-1 and Xsg-7 (P_3)

Of 79 analyses on 78 detrital zircons grains, 74 were concordant for the conglomerate matrix sample Xsg-1. The measured ages are between 2592 Ma and 280 Ma, with major age groups at 330–300 Ma, 360–340 Ma, and 475–430 Ma, and subordinate age groups at 850–760 Ma, 1500–1400, and 2600–2400 Ma (Fig. 7I). Minor other ages scatter at ca. 280, 400, 650–500, and 1200–1000 Ma.

Fourteen analyses of 14 zircon grains were undertaken on the granitic gneiss clast sample Xsg-7. Fourteen analyses provided concordant ages, ranging from 802 Ma to 760 Ma and forming two groups on the concordia diagram (Fig. 8I). The older group consists of seven analyses mostly from the core regions of grains (Supplementary Fig. S1 [see footnote 1]), and it fives a mean age at 799 ± 8 Ma (2σ), with a MSWD value of 0.08 (Fig. 8I). The other seven zircons present prismatic euhedral crystals and clearly oscillatory zoning (Supplementary Fig. S1 [see footnote 1]) and give a weighted mean $^{206}Pb/^{238}U$ age of 770 ± 6 Ma (2σ), with a MSWD value of 0.68 (Fig. 8I).

Zircon Trace Elements

The chemical compositions of 366 detrital zircon grains from clastic rocks and 60 magmatic zircon grains from volcanic clasts with ages younger than 542 Ma are presented in Supplementary Table S3 (see footnote 1). Most of the analyzed grains have REE patterns that increase steeply from La to Lu, with positive Ce anomalies and negative Eu anomalies (Figs. 9A, 9B, and 9C). The geochemistry of zircon provides a sensitive monitor of its parental magma composition and is effective for fingerprinting tectono-magmatic provenance (Grimes et al., 2015). All zircons were plotted on Th/Nb versus Hf/Th diagrams (Figs. 9D, 9E, and 9F) to examine the nature of the source magma from which they crystallized (J.H. Yang et al., 2012). The majority of the Paleozoic zircons lie in the arc-related/orogenic field, with a few grains falling into the within-plate/anorogenic fields (Figs. 9D, 9E, and 9F).

Zircon Lu-Hf Isotopes

Zircon Lu-Hf isotopic data are presented in Supplementary Table S4 (see footnote 1) and are illustrated in Figure 10. Considering that Precambrian zircons are only a minor component of the age spectrum of the analyzed samples, only zircons with U-Pb ages younger than 500 Ma from 252 grains were analyzed. Most zircons with ages younger than 400 Ma displayed positive $\varepsilon_{Hf}(t)$ values (+1 to +14), whereas zircons with ages of 500–400 Ma exhibited a large range of $\varepsilon_{Hf}(t)$ values from –11 to +15.

DISCUSSION

Constraint on Depositional Ages

Although the depositional age of the late Paleozoic strata in the Yili block has been partly constrained based on microfossils, further studies are required, especially for strata where index fossils are absent. Detrital zircons constrain the maximum depositional age. If the sediments are derived from a volcanic terrane undergoing continuous magmatism, then the youngest U-Pb age can also be taken to approximate the depositional age of the strata (Cawood and Nemchin, 2001; Dickinson and Gehrels, 2009; Wu et al., 2010; Tucker et al., 2013; Y.G. Han et al., 2015). Many different methods have been applied to determine the maximum depositional age of strata using U-Pb ages of detrital zircons (Dickinson and Gehrels, 2009; Jones et al., 2009). Dickinson and Gehrels (2009) concluded that the weighted mean ages of youngest cluster of two or more grain ages ($n \geq 2$) overlapping in age at 1σ (YC1σ [2+]) are more consistently compatible with depositional ages, especially for strata

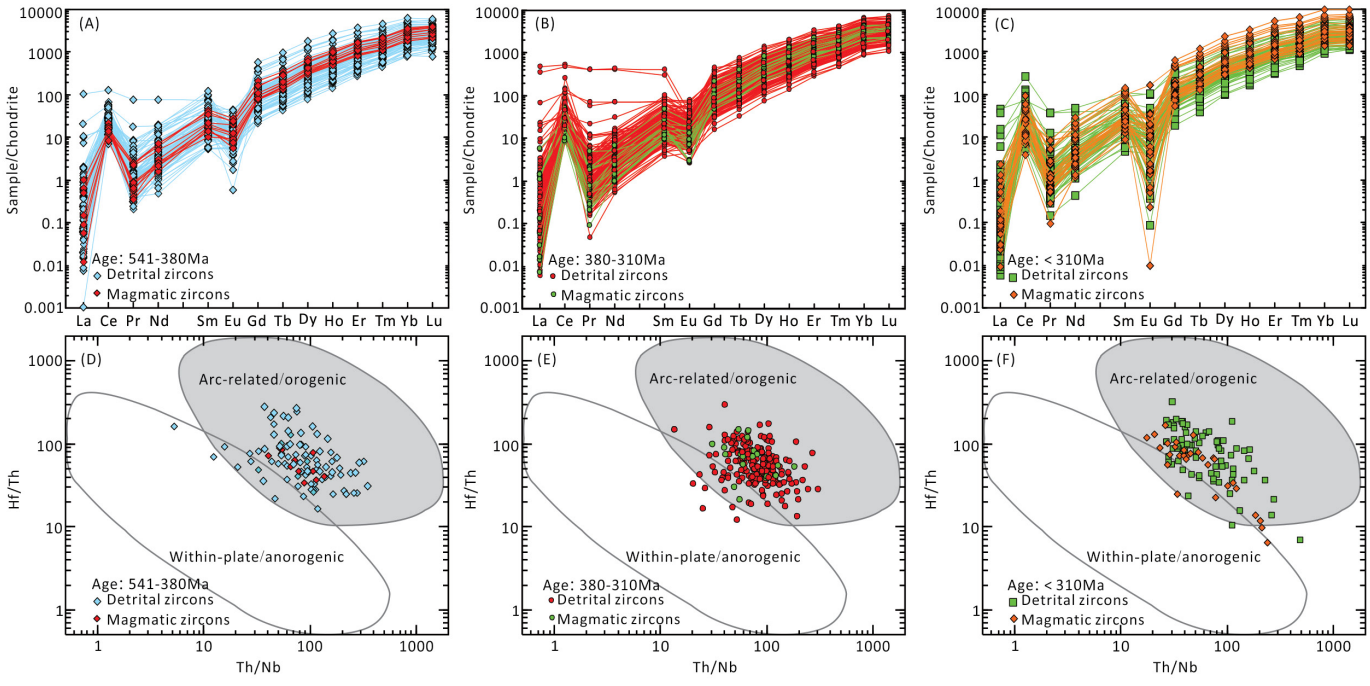

Figure 9. (A–C) Chondrite-normalized rare earth element (REE) patterns and (D–F) Th/Nb vs. Hf/Th diagrams (J.H. Yang et al., 2012) for Paleozoic zircons from the late Paleozoic samples in the Yili Basin. Normalized values for chondrite are from Sun and McDonough (1989).

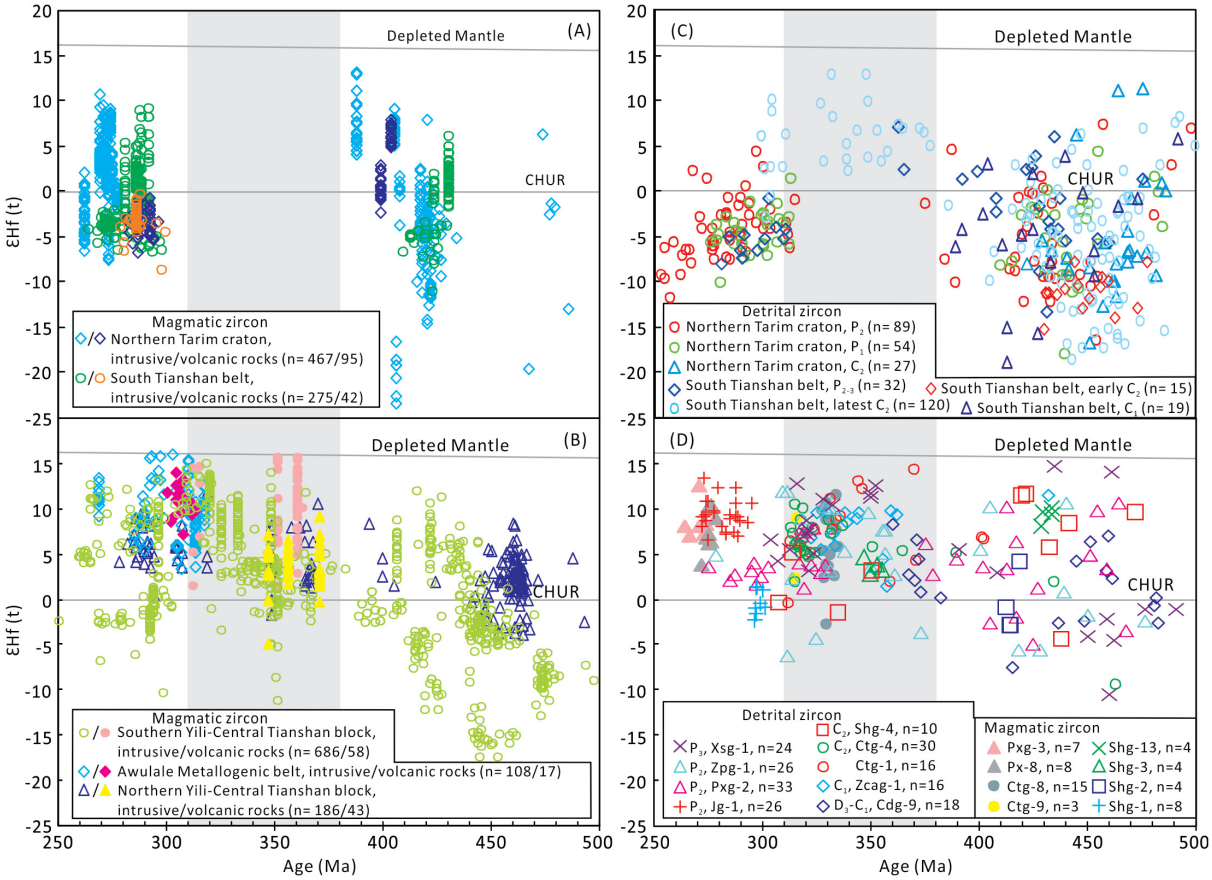

Figure 10. Plots of $\varepsilon_{Hf}(t)$ vs. U-Pb ages for (A) magmatic zircons from the northern Tarim craton and South Tianshan belt, (B) magmatic zircons from the southern Yili–Central Tianshan block, Awulale metallogenic belt, and northern Yili–Central Tianshan block), (C) detrital zircons from the late Paleozoic strata in the northern Tarim craton and South Tianshan belt, and (D) detrital zircons from the Yili Basin. See Figure 2 for abbreviations. Sources of magmatic zircon data: Northern Tarim craton—Han et al. (2016a, and references therein); South Tianshan belt—Han et al. (2016a, and references therein); Southern Yili–Central Tianshan block—D. Li et al. (2015), Gou and Zhang (2016), Han et al. (2016a, and references therein); Awulale metallogenic belt—N.B. Li et al. (2015b), Yan et al. (2015), Han et al. (2016a, and references therein); Northern Yili–Central Tianshan block—An et al. (2017), Han et al. (2016a, and references therein). Sources of detrital zircon data: Northern Tarim craton—Zou et al. (2013), Y.G. Han et al. (2015, 2016a), Z. Li et al. (2015); South Tianshan belt—Han et al. (2016a, 2016b). CHUR—chondritic uniform reservoir; Pt_2—Mesoproterozoic; D_3-C_1—Late Devonian–early Carboniferous; C_1—early Carboniferous; C_2—late Carboniferous; P_1—Early Permian; P_2—Middle Permian; P_3—Late Permian.

derived from contemporaneous volcanic rocks. They also noticed that the youngest single grain ages (YSG) were mostly within 5 m.y. of the depositional ages for ~60% of their samples. In this study, we adopted the YC1σ (2+) age as the most robust age, as well as accepting the YSG age as constraining the maximum depositional age of different units and to approximate the age of strata.

The Dahalajunshan Formation is considered to have accumulated in the early Carboniferous (B. Wang et al., 2007). However, the zircon U-Pb ages of basaltic andesite and rhyolite samples from the lower part of the Dahalajunshan Formation in the northern Tekesi area are 361.3 ± 5.9 Ma and 364.0 ± 3.4 Ma, respectively (Zhu et al., 2009; Yu et al., 2016). This implies that the Dahalajunshan Formation may have formed during the Late Devonian (Cohen et al., 2013). Sample Cdg-9 from the lowermost part of the Dahalajunshan Formation has a youngest single zircon age (YSG) of 360 ± 5 Ma and youngest mean age (YC1σ [2+]) of 367.4 ± 4.2 Ma (Table 1). The maximum depositional age is estimated at ca. 367 Ma. Combined with the zircon U-Pb age of 358.9 ± 2.3 Ma from the basaltic andesites overlying the sandstones and conglomerates (Li et al., 2012), the depositional age of conglomerates from the lowermost part of the Dahalajunshan Formation is restricted to the Late Devonian to earliest Early Carboniferous based on the time scale of Cohen et al. (2013). The Akeshake Formation is considered to have been deposited in the early Carboniferous, based on microfossils. The youngest single zircon age (YSG) and youngest mean age (YC1σ [2+]) of sample Zcag-1 from the lowermost part of the Akeshake Formation are 320 ± 4 Ma and 325.4 ± 2.6 Ma, respectively. This indicates that the Akeshake Formation has a maximum depositional age of late early Carboniferous.

The strata of the Dongtujinhe Formation in the northern Tekesi area were previously classified as part of the Akeshake Formation (B. Wang et al., 2007). However, fossils including

TABLE 1. SUMMARY OF STRATIGRAPHICAL UNIT, AGE, LITHOLOGY, DETRITAL MODES, AND DETRITAL ZIRCON U-Pb AGES OF THE PEBBLY SANDSTONE, CONGLOMERATE MATRIX, AND SANDSTONE CLAST SAMPLES, YILI BASIN, CHINA

Sample	Stratigraphic unit and age		Lithology	No. of valid (all) U-Pb analyses	Youngest age (Ma)	
					YSG*	YC1σ(2+)† (no. of analyses, MSWD)
Xsg-1	Basiergan	P_3	Conglomerate matrix	74 (79)	278 ± 4	
Zpg-1	Tamuqisayi	P_2	Conglomerate matrix	71 (77)	279 ± 5	280.2 ± 7.3 (2, 0.13)
Pxg-2	Tamuqisayi	P_2	Conglomerate matrix	81 (84)	270 ± 4	272.6 ± 6.6 (2, 0.62)
Jg-1	Xiaoshansayi	P_2	Pebbly sandstone	54 (77)	272 ± 4	273.5 ± 2.6 (13, 0.07)
Shg-4	Keguqinshan	C_2	Pebbly sandstone	102 (106)	307 ± 5	311.7 ± 5.3 (2, 1.3)
Ctg-4	Dongtujinhe	C_2	Sandstone clast of conglomerate	81 (83)	311 ± 4	313.0 ± 2.4 (13, 0.10)
Ctg-1	Dongtujinhe	C_2	Pebbly sandstone	58 (75)	311 ± 4	313.1 ± 2.8 (9, 0.09)
Zcag-1	Akeshake	C_1	Pebbly sandstone	63 (65)	320 ± 4	325.4 ± 2.6 (13, 0.61)
Cdg-9	Dahalajunshan	D_3C_1	Conglomerate matrix	63 (71)	360 ± 5	367.4 ± 4.2 (9, 1.20)

Note: P_3—Late Permian, P_2—Middle Permian, C_2—Late Carboniferous, C_1—Early Carboniferous, D_3—Late Devonian. MSWD—mean square of weighted deviates.
*YSG—youngest single detrital zircon age with 1σ uncertainty.
†YC1σ(2+)—weighted mean age (±1σ, incorporating both internal analytical error and external systematic error) of youngest cluster of two or more grain ages ($n \geq 2$) overlapping in age at 1σ. The actual numbers of grains included in YC1σ(2+) grain clusters vary upward to a maximum of 13 (Dickinson and Gehrels, 2009).

the bivalves *Aviculopecten occidentalis* Shumard, *Streblochondria tenuilineata* (Meek and Worthen), *Palaeoneilo anthraconeiloides* (Chao), *Wilkingia* cf. *regularis* (King), Brachiopoda *Dielasma bovidens* Morton, and the plant *Noeggerathiopsis* sp. have been reported from mudstones in the upper part of this section (Zhang et al., 2006). According to the biostratigraphic correlation, these sedimentary sequences should be classified as part of the Dongtujinhe Formation and were deposited in the late Carboniferous (Zhang et al., 2006). The youngest mean age (YC1σ [2+]) from the pebbly sandstone sample Ctg-4 is 313.0 ± 2.4 Ma, with a youngest single zircon age (YSG) of 311 ± 4 Ma, similar to that of the sandstone clast sample Ctg-1 (Table 1). These age data indicate that deposition of the Dongtujinhe Formation must have commenced after ca. 313 Ma.

Fossils from the Keguqinshan Formation near the Tekesi area indicate that it was deposited at the end of the late Carboniferous (Y.J. Li et al., 2011). The youngest mean age (YC1σ [2+]) from the pebbly sandstone sample Shg-4 is 311.7 ± 5.3 Ma, with a youngest single zircon age (YSG) of 307 ± 5 Ma (Table 1). Combined with the zircon U-Pb age of 299.0 ± 1.7 Ma from granitic clast sample Shg-1, these data indicate that the Keguqinshan Formation could have been deposited at the end of the Carboniferous (ca. 300 Ma).

The age of the Xiaoshansayi Formation is poorly constrained, due to the lack of index fossils. The zircon U-Pb age of granites intruding the formation at Nileke is 269 ± 3 Ma (Li et al., 2013), providing an upper time limit for the depositional age. The youngest mean age (YC1σ [2+]) from pebbly sandstone sample Jg-1 is 273.5 ± 2.6 Ma, consistent with the youngest single zircon age (YSG = 272 ± 4 Ma), and the maximum depositional age of the Xiaoshansayi Formation is estimated at ca. 273 Ma. These age data indicate that the Xiaoshansayi Formation accumulated in the earliest Middle Permian.

The depositional age of the Tamuqisayi Formation has been restricted to the Middle Permian, based on fossils including plants *Prynadaeopteris anthriscifolia* and *P. glossitiformis* (Song et al., 2005). The youngest mean age (YC1σ [2+]) and youngest single zircon age (YSG) from sample Pxg-2 are 272.6 ± 6.6 Ma and 270 ± 4 Ma, respectively (Table 1), consistent with the weighted mean $^{206}Pb/^{238}U$ age of 271.9 ± 2.5 Ma from andesite clast sample Pxg-3. Consequently, the maximum depositional age of the Tamuqisayi Formation is estimated at ca. 272 Ma. However, the youngest mean age (YC1σ [2+]) and youngest single zircon age (YSG) from sample Zpg-1 are 279 ± 5 Ma and 280.2 ± 7.3 Ma, respectively (Table 1), and the maximum depositional age is estimated at ca. 280 Ma. This estimated age is older than that from sample Pxg-2 and biostratigraphic studies. Similarly, the youngest single zircon age (YSG) from the Basiergan Formation sample Xsg-1 is 278 ± 4 Ma (Table 1), which is older than the well-constrained Late Permian biostratigraphic age (Song et al., 2005). This difference may be attributed to the termination of magmatism during the Late Permian in the Tianshan region (Fig. 11) and no input of contemporaneous volcanic materials into the depocenter.

Sedimentary Provenance

The ages of magmatism in the Yili–Central Tianshan block, South Tianshan belt, and Tarim craton were summarized by Han et al. (2016a). These units are potential source terranes for the sedimentary sequence. In this study, the Yili–Central Tianshan block is further divided into the southern Yili–Central Tianshan block, northern Yili–Central Tianshan block, and Awulale metallogenic belt to display the age data on the distribution of magmatism (Fig. 11). Magmatism in the Tarim craton occurred at 300–270 Ma, 430–390 Ma, 1.1–0.6 Ga, 1.9–1.7 Ga, and ca. 2.5 Ga, with an additional minor pulse at ca. 460 Ma. The South Tianshan belt has similar magmatic episodes to the Tarim craton, except for the absence of ca. 460 Ma and Precambrian magmatic rocks. Compared with the Tarim craton, the Yili–Central Tianshan block shows evidence for a unique and abundant magmatic pulse at 380–310 Ma (Han et al., 2016a; Fig. 11). Furthermore, the magmatic rocks with ages of 520–470 Ma and 1.4–1.1 Ga are only present in the southern Yili–Central Tianshan block (Fig. 11C). Magmatic rocks in the interval 340–320 Ma are absent from the northern margin of the Yili–Central Tianshan block but are abundant in the Awulale metallogenic belt and the southern Yili–Central Tianshan block (Fig. 11).

Most 500–400 Ma magmatic zircons in the Tianshan region have $\varepsilon_{Hf}(t)$ values between –15 and +10 (Figs. 10A and 10B). The Permian zircons from the intrusive rocks both in the northern Tarim craton and South Tianshan belt have $\varepsilon_{Hf}(t)$ values ranging from –8 to +10, whereas those from the volcanic rocks only show negative $\varepsilon_{Hf}(t)$ values (Fig. 10A). Most magmatic zircons with ages younger than 380 Ma in the Yili–Central Tianshan block have positive $\varepsilon_{Hf}(t)$ values (Fig. 10B), and only some Permian zircons from the intrusive rocks in the southern part of the block show negative $\varepsilon_{Hf}(t)$ values (Fig. 10B).

Provenance of Late Devonian to Carboniferous Successions

The 460–430 Ma, 505–480 Ma, and Mesoproterozoic to Neoproterozoic detrital zircons are abundant in sample Cdg-9, consistent with the magmatic record in the southern Yili–Central Tianshan block (Fig. 11C; Li et al., 2009; Alexeiev et al., 2011; De Grave et al., 2011; Zhu, 2012; Kröner et al., 2013; X.Y. Xu et al., 2013). This supports the interpretation that clasts from conglomerates of the Dahalajunshan Formation were derived from the underlying volcano-sedimentary strata in the southern

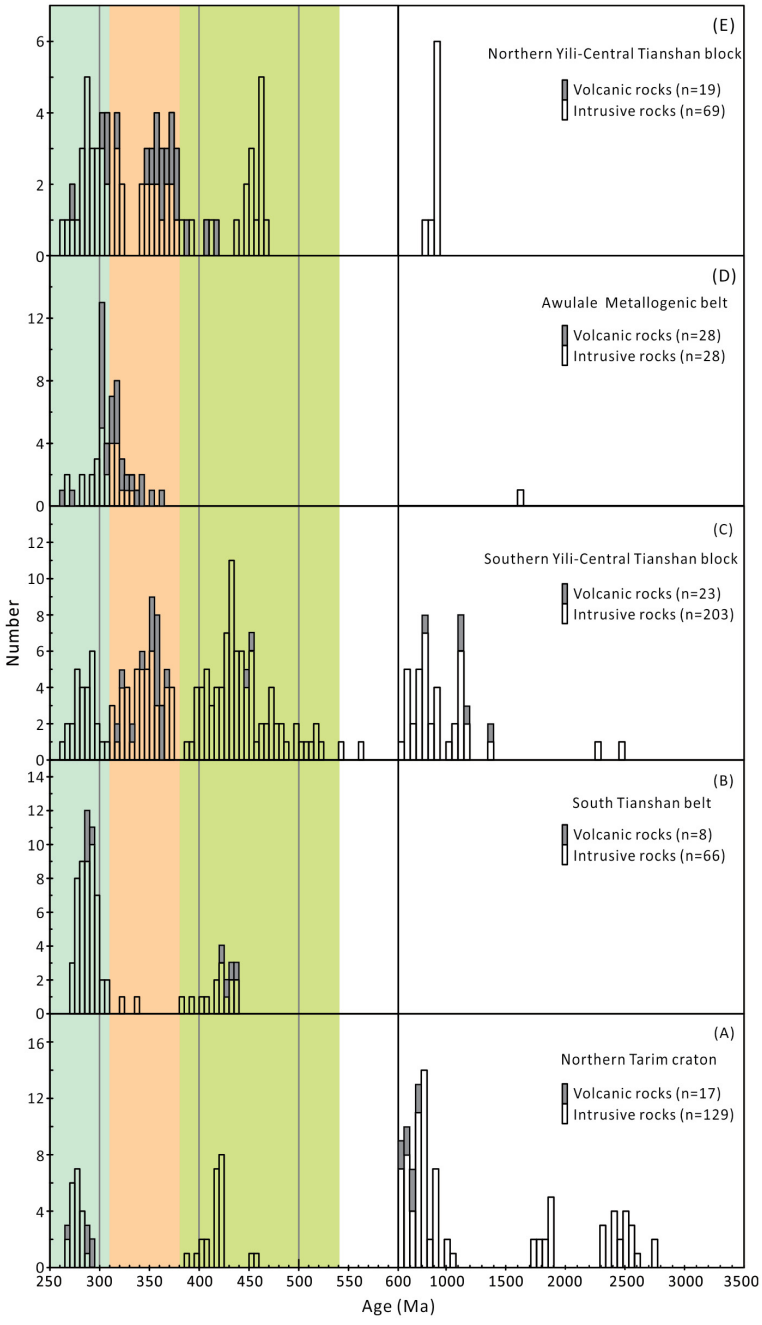

Figure 11. Histograms for compiled crystallization ages of magmatic rocks in the Tarim craton and Tianshan regions. Note that the bin widths of the histograms are 5 m.y. for ages younger than 600 Ma and 50 m.y. for ages older than 600 Ma. The *x*-axis scales are different for portions younger than 600 Ma and older than 600 Ma. Sources of data: Northern Tarim craton—Han et al. (2016a, and references therein); South Tianshan belt—Han et al. (2016a, and references therein); Southern Yili–Central Tianshan block—D. Li et al. (2015), Gou and Zhang (2016), Han et al. (2016a, and references therein); Awulale metallogenic belt—Li et al. (2009), N.B. Li et al. (2015b), Q. Han et al. (2015), Y.G. Han et al. (2016a, and references therein), Yan et al. (2015), Zhang et al. (2015); Northern Yili–Central Tianshan block—B.F. Han et al. (2010), Y.G. Han et al. (2016a, and references therein), Zhao et al. (2014), C. Li et al. (2015), An et al. (2017), Yu et al. (2016).

Yili–Central Tianshan block (Xia et al., 2012). The 380–360 Ma zircon grains are euhedral/prismatic, with clear oscillatory zoning and high Th/U ratios, indicative of derivation from nearby sources. Late Devonian volcanic rocks have been reported around the Tekesi area (Zhu et al., 2009; Yu et al., 2016) and are the inferred source of these grains. The northern margin of the Yili–Central Tianshan block also has abundant Late Devonian magmatic rocks (An et al., 2013; Yu et al., 2016). However, the equivalent sandstones in the northern Yili block include 410–390 Ma detrital zircons with a peak at 405 Ma (H.S. Liu et al., 2014), which are absent from sample Cdg-9 (Fig. 7A), suggesting a restricted source. Detrital zircons with ages younger than 500 Ma show similar Hf isotopic signatures as the contemporaneous magmatic zircons in the southern Yili–Central Tianshan block. Thus, we conclude that conglomerates of the Dahalajunshan Formation were mainly derived from the underlying strata and contemporaneous volcanic rocks in the southern Yili–Central Tianshan block.

The U-Pb detrital zircon age distribution of Akeshake Formation sample Zcag-1 is characterized by a single age population with an early Carboniferous age peak at ca. 336 Ma. Magmatic rocks in the range 340–320 Ma are only distributed in the southern Yili–Central Tianshan block and Awulale metallogenic belt (Zhu et al., 2009; Yu et al., 2016). In combination with the northwestward paleocurrents, the southern Yili–Central Tianshan block is the likely major source of detritus. Furthermore, the presence of abundant lathwork and microlitic volcanic lithic fragments in the sandstones and basaltic clasts in the conglomerate indicates a basaltic volcanic source for the Akeshake Formation sediments.

Detrital zircons from a sandstone clast (sample Ctg-1) within a conglomerate near the base of the Dongtujinhe Formation show a similar age spectrum (Figs. 7C and 7D) and Hf isotopic signatures as those from the pebbly sandstone sample Ctg-4 (Fig. 10D). The zircon U-Pb age of andesite clast sample Ctg-9 is 316.2 ± 2.4 Ma, corresponding to the age of the Yishijilike Formation volcanic rocks (313 ± 3 Ma; Bai et al., 2015a). Together with the unconformable contact between the Dongtujinhe Formation and Yishijilike Formation, this suggests that detritus in the Dongtujinhe Formation includes materials reworked from the Yishijilike Formation. The presence of a rhyolite clast with an age of 331.5 ± 2.0 Ma suggests that the Dahalajunshan Formation volcanic rocks in the southern Yili–Central Tianshan block also acted as a source for detritus. Neoproterozoic (880–740 Ma) detrital zircons in samples Cdg-1 and Cdg-4 correspond with the ages of metamorphic and magmatic rocks occurring across the Yili–Central

Tianshan block (B. Wang et al., 2014a, 2014b; Gao et al., 2015; Z. Huang et al., 2015). Considering that all analyzed Neoproterozoic detrital zircon grains are euhedral/prismatic, with clear oscillatory zoning and high Th/U ratios, they were likely derived from nearby sources. The contact relationship between the Dongtujinhe Formation and Yishijilike Formation is unconformable at Tekesi (Fig. 3), but it is conformable at Nileke (Bai et al., 2015a). The sandstone and volcanic clasts decrease in size and abundance from the Tekesi section toward the Nileke section (Bai et al., 2015a). These data indicate that the detritus in the Dongtujinhe Formation was mainly derived from the southern Yili–Central Tianshan block.

Detrital zircons from the pebbly sandstone sample Shg-4 from the Keguqinshan Formation are distinguished from the Dongtujinhe Formation by the presence of abundant early Paleozoic and Precambrian detrital grains (Fig. 7E). Combined with the northwestward paleocurrents, the southern Yili–Central Tianshan block, South Tianshan belt, and Tarim craton are potential source terranes for the Keguqinshan Formation. The detrital zircon age spectrum (Fig. 7E) and magmatic zircon ages from granitic clasts (Figs. 8C, 8D, 8E, and 8F) are consistent with magmatic episodes in the southern Yili–Central Tianshan block (Fig. 11C). Zircons with ages younger than 500 Ma also show similar Hf isotopic signatures as the contemporaneous magmatic zircons in the southern Yili–Central Tianshan block (Figs. 10B and 10D). These signatures indicate that the southern Yili–Central Tianshan block was an important source of detritus. However, the presence of abundant eclogite clasts indicates that the (U)HP metamorphic belt in the northern South Tianshan belt also acted as a source. Furthermore, the age spectrum of detrital zircons from the Keguqinshan Formation at Tekesi shows overall similarities to that from coeval strata in the South Tianshan belt (Han et al., 2016b; see also Figs. 12H and 12M). This supports the interpretation that a positive topographic highland may have been present between the southern Yili–Central Tianshan block and South Tianshan belt and acted as the main source for detritus in the southern Yili Basin.

Provenance of Middle–Late Permian Successions

The pebbly sandstone sample Jg-1 from the Xiaoshansayi Formation at Nileke is dominated by Early Permian detrital zircons with a single peak at 278 Ma. Magmatic rocks with this age are widely reported in the Tianshan region (Fig. 11). However, the Early Permian zircons from the volcanic rocks in the northern Tarim craton and South Tianshan belt have negative $\varepsilon_{Hf}(t)$ values, which are different from the detrital zircons in sample Jg-1(mostly +6 to +14). This indicates that the detritus in the Xiaoshansayi Formation was unlikely to have been derived from the northern Tarim craton and South Tianshan belt. Importantly, the analyzed zircon grains have a euhedral/prismatic shape and show clear oscillatory zoning with high Th/U ratios, suggesting a nearby magmatic source. The outcrop area of the Early Permian volcanic rocks in the northern Yili–Central Tianshan block is limited (Wang et al., 2009), and it is unlikely that they alone could have provided the abundant 300–270 Ma detritus. Early Permian volcanic rocks are extensively exposed at Nileke and north of Tekesi (Fig. 2). Importantly, Middle Permian strata are unconformable on late Carboniferous strata in the southern Yili–Central Tianshan block (Wang et al., 2009). A positive topographic highland is inferred in the southern Yili–Central Tianshan block (Liu et al., 2013) and likely was a main source for detritus.

The conglomerate matrix samples (Zpg-1 and Pxg-2) from the Tamuqisayi Formation are distinguished from the Xiaoshansayi Formation by the presence of abundant pre-Permian detrital grains (Figs. 7G, 7H, and 7I). Detrital zircons with ages of 390–310 Ma are abundant in these samples, but coeval magmatic rocks and detrital zircons with these ages from equivalent sequences in the South Tianshan and Tarim regions are almost absent (Figs. 11 and 12). Outcrop and borehole data show the Tamuqisayi Formation in the southern Yili–Central Tianshan block unconformably underlies Silurian to Carboniferous volcano-sedimentary successions (B. Wang et al., 2007; C. Li et al., 2015). Combined with the similar Hf isotopic signatures (Fig. 10), the Paleozoic sedimentary-volcano successions in the southern Yili–Central Tianshan block are the likely main source for detritus. Compared with sample Zpg-1 at Zhaosu, the conglomerate matrix sample Pxg-2 at Nileke shows more Early–Middle Permian detrital grains, consistent with the presence of Early–Middle Permian volcanic clasts. This indicates that the Early–Middle Permian sedimentary-volcano rocks may have been exposed near the Nileke area, whereas the Zhaosu area was closer to the main source in the southern Yili-Central Tianshan block where sedimentary-volcano rocks with these ages may have been eroded. Precambrian detrital grains with a single peak at 830 Ma are present in sample Zpg-1 (Fig. 7H), but they are nearly absent in sample Pxg-2. This indicates that the Precambrian basement may have been exposed in the southern Yili–Central Tianshan block and acted as a source for adjacent detritus.

Age spectrum and Hf isotopic signatures of detrital zircons in the conglomerate matrix sample Xsg-1 from the Basiergan Formation at Nileke show overall similarities to those from the Tamuqisayi Formation at Zhaosu (Figs. 7H, 7I, and 10). In combination with the north-northeastward paleocurrents, this suggests that the Late Permian clastic rocks at Nileke were mainly derived from the southern Yili–Central Tianshan block. The proportion of 1.5–1.1 Ga and 2.6–2.4 Ga detrital zircons increases from the Middle Permian to the Late Permian succession (Fig. 7), indicating increasing input from the basement in the southern Yili–Central Tianshan block. The granitic gneiss clasts from the Xiaoshansayi Formation have similar magmatic ages to those recorded in the granitic gneisses from the Central Tianshan block (Z. Huang et al., 2015), supporting this interpretation.

Considering that the Awulale metallogenic belt is parallel to, and close to, the North Tianshan belt (Fig. 1B), we cannot rule out the possibility that the northern Yili–Central Tianshan block may have been the source for Permian detritus at Nileke. However, paleocurrent directions suggest sediment transport from the south to the north (Fig. 3). Meanwhile, detrital zircons from the Permian sedimentary rocks in the Awulale metallogenic belt and southern Yili–Central Tianshan block have similar age spectra and Hf isotopic signatures. Detrital zircon data from the Permian sandstones show sediments supplied along the North Tianshan belt were partly derived from the Central Tianshan block, implying a widening of the drainage system toward the southern Yili–Central Tianshan block (W. Yang et al., 2013). Furthermore, the timing of magmatic episodes in the Awulale metallogenic belt and southern Yili–Central Tianshan block are similar, and contrast with those in the northern Yili–Central Tianshan block (Fig. 11). Therefore, we conclude that the Permian clastic rocks from the Awulale metallogenic belt formed in a similar tectonic environment as those from the southern Yili Basin, and the southern Yili–Central Tianshan block was the likely main source for late Paleozoic detritus in the analyzed samples.

Age of Collision

The time of collision between the Yili–Central Tianshan block and the Tarim craton ranged from Late Devonian to Middle Triassic (e.g., Xia et al., 2008; Han et al., 2011; H. Huang et al., 2015; Zhang et al., 2007). The model showing that final collision along the South Tianshan region terminated in the Late Devonian–early Carboniferous is mainly based on the regional

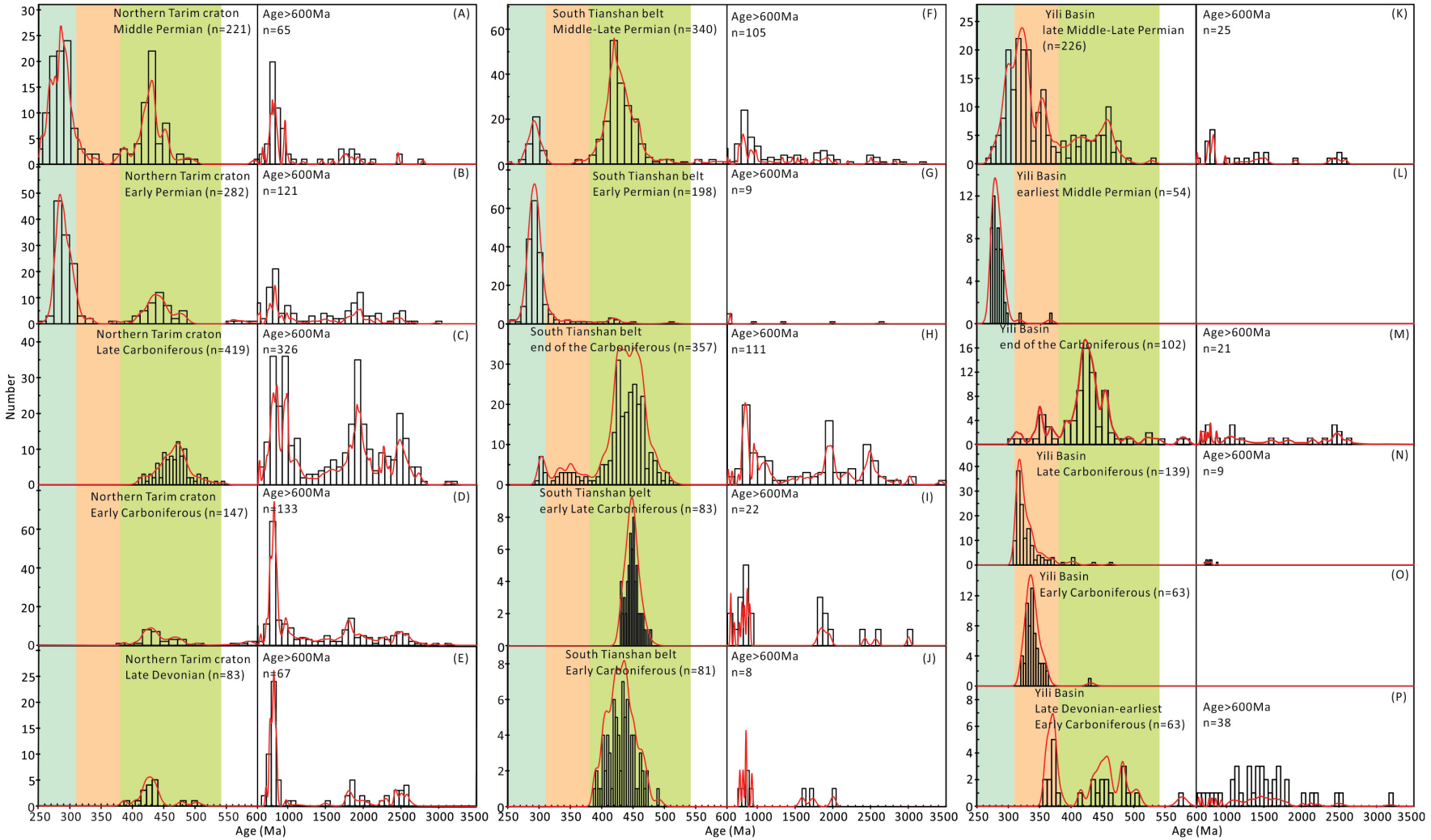

Figure 12. Histograms and probability curves comparing analyzed detrital zircons models in late Paleozoic succession from the Yili Basin (this study), northern Tarim craton (Zou et al., 2013; Y.G. Han et al., 2015, 2016a; Z. Li et al., 2015), and South Tianshan belt (Carroll et al., 2013; Liu et al., 2013; Han et al., 2016a, 2016b). The *x*-axis scales are different for portions younger than 600 Ma and older than 600 Ma. The *y* axes for portions younger than 600 Ma are expanded to highlight the Paleozoic zircon populations.

unconformity at the base of the Dahalajunshan Formation (Xia et al., 2008, 2012; Charvet et al., 2011; X.Y. Xu et al., 2013; Bai et al., 2015a). The Carboniferous volcanic rocks in the Yili–Central Tianshan block were proposed to have formed in an intracontinental rift setting and be related to plume-derived magmatism (Xia et al., 2008, 2012; X.Y. Xu et al., 2013). The arc-like signatures of the Carboniferous volcanic rocks are interpreted to result from crustal contamination (Xia et al., 2008, 2012). However, this model is inconsistent with the presence of late early Carboniferous ophiolites in both the North and South Tianshan belts (Xu et al., 2006; T. Jiang et al., 2014; C. Li et al., 2015). All 380–310 Ma zircons have Th/Nb >10 (Fig. 9E), suggesting that Carboniferous volcanic rocks possibly formed with some crustal contamination (Yang et al., 2015; Huang et al., 2016). However, on the Th/Nb-Hf/Th diagram (J.H. Yang et al., 2012; Fig. 9E), the trace-element trends of these zircons are indicative of crystallization from arc-related/orogenic magmas. This indicates that Carboniferous magmatic rocks in the Yili–Central Tianshan block were unlikely to have formed in a plume-related environment, and this supports the interpretation that these magmatic rocks were generated in a continental arc setting (Zhu et al., 2009; Gou et al., 2012; Yu et al., 2016; Zhang et al., 2015).

The U-Pb age spectra of detrital zircons clearly indicate that there are no zircons younger than 264 Ma in the Permian strata, and this is consistent with previous work on detrital zircons from the Tekesi River and its southern branches flowing through the northern slope of the South Tianshan orogenic belt (Ren et al., 2011). These data imply that the major magmatic events in the Southern Tianshan orogenic belt and Yili–Central Tianshan block occurred mainly in the Paleozoic, and these areas lack a record of Late Permian and younger magmatism. Thus, the South Tianshan orogenic belt likely formed prior to this time. The stratigraphic synthesis suggests that the Carboniferous strata in the South Tianshan belt are characterized by marine deposits (Han et al., 2016a), compared with the terrigenous clastic rocks, shallow-marine carbonate successions, and volcanic rocks in the southern Yili–Central Tianshan block. These successions are overlain by Permian continental deposits and volcanic rocks in the southern Yili–Central Tianshan block and South Tianshan belt (B.F. Han et al., 2011; Y.G. Han et al., 2016a; D.D. Liu et al., 2013, 2014; this study). This regional sedimentary variation from the Carboniferous to Permian records is consistent with collision between the Tarim craton and Yili–Central Tianshan block occurring prior to the Permian.

Recent robust radiometric dating indicated that peak eclogite-facies metamorphism along the subducted northern margin of the Tarim craton occurred at 320–310 Ma (Fig. 13; Hegner et al., 2010; Su et al., 2010; Klemd et al., 2011; X. Yang et al., 2013; X. Liu et al., 2014). Rb/Sr and $^{40}Ar/^{39}Ar$ dating of retrograde eclogites and blueschists indicates that the (U)HP metamorphic rocks experienced exhumation mainly between 320 Ma and 310 Ma (Fig. 13; Klemd et al., 2005; Hegner et al., 2010; Xia et al., 2016). These ages for the formation and exhumation of metamorphic rocks indicate that the collision between the Tarim craton and Yili–Central Tianshan block mostly took place during the late Carboniferous.

The ages of arc-related volcanic rocks in the Yishijilike Formation (Zhu et al., 2009; Bai et al., 2015a) indicate that subduction of the South Tianshan Ocean may have continued to at least ca. 313 Ma, based on data from samples Ctg-4, Ctg-1, and Ctg-9, and from underlying arc-related volcanic rocks of the Yishijilike Formation (Zhu et al., 2009; Bai et al., 2015a). Combined with the biostratigraphic age constraints (Zhang et al., 2006), this implies that the age gap across the unconformity between the Dongtujinhe Formation and Yishijilike Formation at Tekesi may be very short, and, thus, the age of uplift in the southern Yili–Central Tianshan block is constrained to ca. 310 Ma. This age is consistent with the youngest ages of tectonic exhumation of South Tianshan (U)HP metamorphic rocks (Hegner et al., 2010; Su et al., 2010; Xia et al., 2016) and the age of deformation in the ophiolite mélanges and metamorphic belt (Alexeiev et al., 2015). The unconformity at the base of the Dongtujinhe Formation possibly records deformation of the overriding plate during the exhumation of (U)HP metamorphic rocks and the terminal stages of oceanic subduction (Li et al., 2016; Soldner et al., 2016). Considering the multiple sources supplying detritus to the clastic rocks of the Dongtujinhe Formation, we interpret ca. 310 Ma as the time of the initial collision between the Tarim craton and Yili–Central Tianshan block. Moreover, Late Devonian–late Carboniferous (380–310 Ma) arc-related magmatic rocks occur widely in the southern Yili–Central Tianshan block (Fig. 11) and were formed by the northward-directed subduction of the South Tianshan Ocean (Zhu et al., 2009; Gou et al., 2012; Yu et al., 2016). However, coeval magmatic rocks are nearly absent in the northern Tarim and South Tianshan regions (Fig. 11). Combined with the similar age spectra and $\varepsilon_{Hf}(t)$ values of detrital zircons (Figs. 10 and 12), the sedimentary successions during the Late Devonian to late Carboniferous in the South Tianshan belt formed on the northern margin of the Tarim craton (Y.G. Han et al., 2015, 2016a). Detrital zircon age and Hf isotopic data show that the Late Devonian to late Carboniferous (380–300 Ma) magmatic rocks from the southern Yili–Central Tianshan block were not the source for the late Paleozoic strata until the end of the Carboniferous (ca. 300 Ma; Figs. 8C and 10; Han et al., 2016a, 2016b). Furthermore, the Early Permian volcanic rocks with ages of 295–285 Ma unconformably overlie strongly folded early and late Carboniferous strata in the South Tianshan orogenic belt (D.D. Liu et al., 2014; H. Huang et al., 2015). Importantly, the latest Carboniferous (304–299 Ma) unmetamorphosed and little-deformed molasse-type conglomerates unconformably overlie (U)HP metamorphic rocks in the Atbashi belt (Hegner et al., 2010). The presence of eclogite clasts in the conglomerate from the Atbashi belt indicates that exhumation and exposure of the (U)HP metamorphic rocks occurred before ca. 300 Ma (Hegner et al., 2010). Abundant eclogite clasts in the conglomerate of the Keguqinshan Formation suggest that (U)HP metamorphic rocks in the South Tianshan belt had been eroded and acted as a source for the detritus in the southern Yili Basin at ca. 300 Ma. These provenance and stratigraphic relationships indicate that the final amalgamation associated with the continent-continent collision between the Tarim craton and Yili–Central Tianshan block probably took place at ca. 300 Ma.

Tectonic Evolution of the South Tianshan Orogenic Belt

The 430–330 Ma ophiolitic rocks discovered in the South Tianshan orogenic belt (Wang et al., 2011; Jian et al., 2013; T. Jiang et al., 2014) indicate that the South Tianshan Ocean was open by at least the Late Silurian and lasted into the early Carboniferous. However, the subduction polarities during the consumption of the South Tianshan Ocean are controversial (e.g., B.F. Han et al., 2011; Y.G. Han et al., 2015, 2016a; Wang et al., 2011; Ge et al., 2014). Although Silurian to Early Devonian magmatic rocks occur widely in the Yili–Central Tianshan, Tarim, and South Tianshan regions, it is clear that Late Devonian to late Carboniferous (380–310 Ma) magmatic rocks are largely absent in the northern Tarim and South Tianshan regions but occur widely in the southern Yili–Central Tianshan block (Figs. 11 and 13). Late Devonian–late Carboniferous clastic rocks in the Yili Basin contain abundant contemporaneous volcanic detritus derived from nearby magmatic arc sources. However, Late Devonian–late Carboniferous (380–310 Ma) detrital zircons are absent in the early Carboniferous to early late Carboniferous

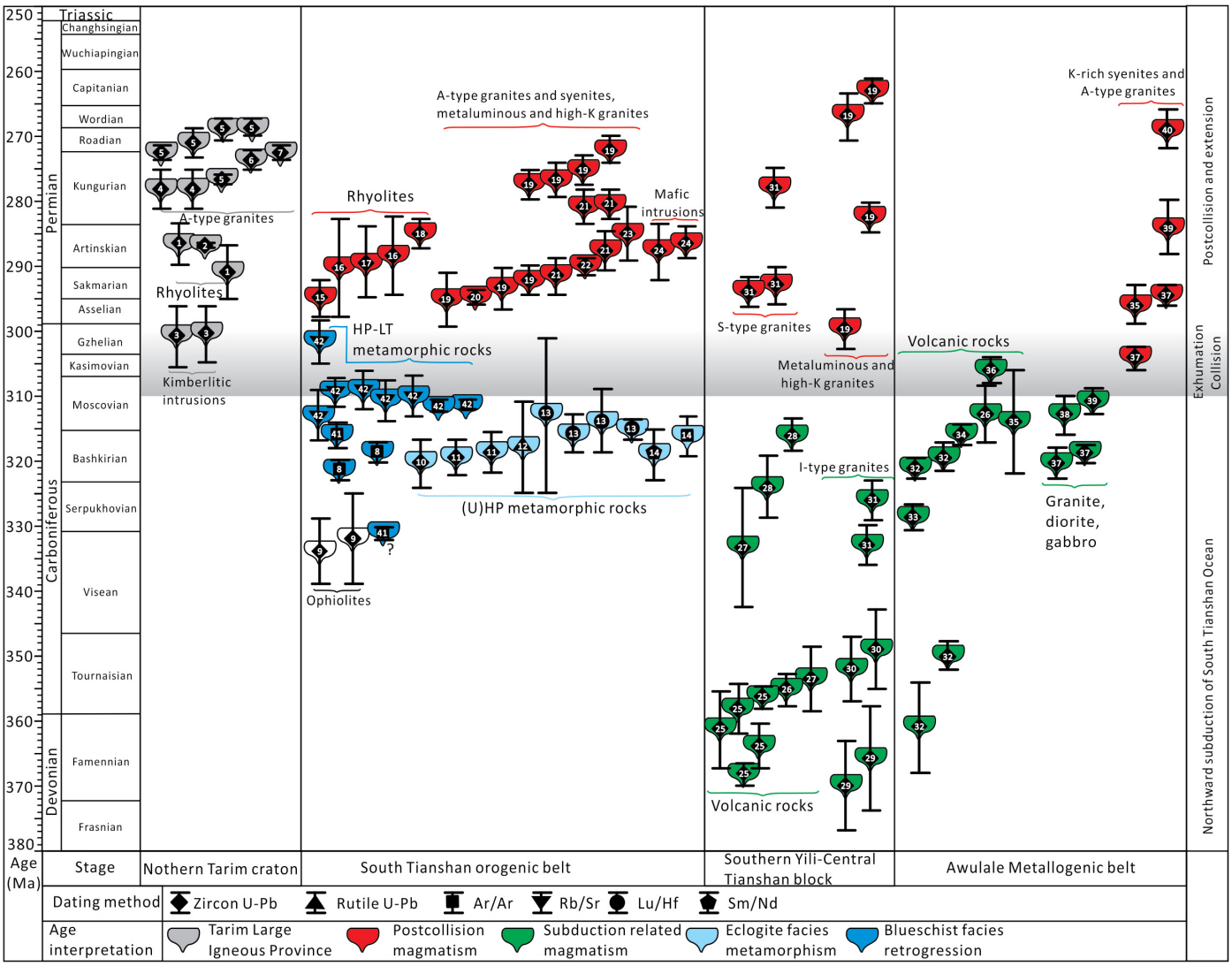

Figure 13. Schematic time-space diagram of magmatic activities and metamorphic events during Late Devonian to Permian evolution of the South Tianshan orogenic belt and adjoining regions. Sources of data: 1—Tian et al. (2010); 2—H.Q. Liu et al. (2014); 3—Zhang et al. (2013); 4—Zhang et al. (2010); 5—Zhang and Zou (2013); 6—Zhang et al. (2008); 7—Huang et al. (2012a); 8—Xia et al. (2016); 9—T. Jiang et al. (2014); 10—X. Yang et al. (2013); 11—Su et al. (2010); 12—Q.L. Li et al. (2011); 13—Klemd et al. (2011); 14—Hegner et al. (2010); 15—D.D. Liu et al. (2014); 16—M. Wang et al. (2014); 17—Luo et al. (2008); 18—H. Huang et al. (2015); 19—X.X. Ma et al. (2015); 20—Yang et al. (2011); 21—C.H. Liu et al. (2014); 22—Huang et al. (2014); 23—Long et al. (2008); 24—Huang et al. (2012b); 25—Zhu et al. (2009); 26—Zhu et al. (2005); 27—Zhu et al. (2010); 28—Yu et al. (2016); 29—Zhu et al. (2006); 30—Gao et al. (2009); 31—Gou et al. (2012); 32—Zhang et al. (2015); 33—Z.S. Jiang et al. (2014); 34—Duan et al. (2014); 35—N.B. Li et al. (2015b); 36—N.B. Li et al. (2015a); 37—Zhang et al. (2012); 38—Yan et al. (2015); 39—W.B. Yang et al. (2012); 40—Li et al. (2013); 41—Wang et al. (2010); 42—Klemd et al. (2005). The time scale is based on Cohen et al. (2013). HP-LT—high-pressure–low-temperature; (U)HP—(ultra)high-pressure.

clastic rocks in both the South Tianshan belt and the northern Tarim craton (Fig. 12). This is consistent with northward oceanic subduction during the Late Devonian to late Carboniferous (380–310 Ma; Fig. 14A). The strong northward subduction of the South Tianshan Ocean may have resulted in regional uplift in the southern Yili–Central Tianshan block during the Late Devonian (Xia et al., 2014). This tectonothermal event corresponds with the regional unconformity at the base of the Dahalajunshan Formation and is consistent with the equivalent southward thrust structures in the Zhaosu-Tekesi areas (D. Li et al., 2015). During the late early Carboniferous, the entire southern Yili–Central Tianshan block was dominated by carbonate and clastic rocks that were mainly deposited in a mixed nearshore to platform-margin reef environment, indicating a relatively stable tectonic setting (D. Li et al., 2015). This interpretation is consistent with a single basaltic volcanic source without any input of detritus from basement for the Akeshake Formation.

During the late Carboniferous (ca. 310–300 Ma), the South Tianshan Ocean finally closed, associated with the collision between the Yili–Central Tianshan block and the Tarim

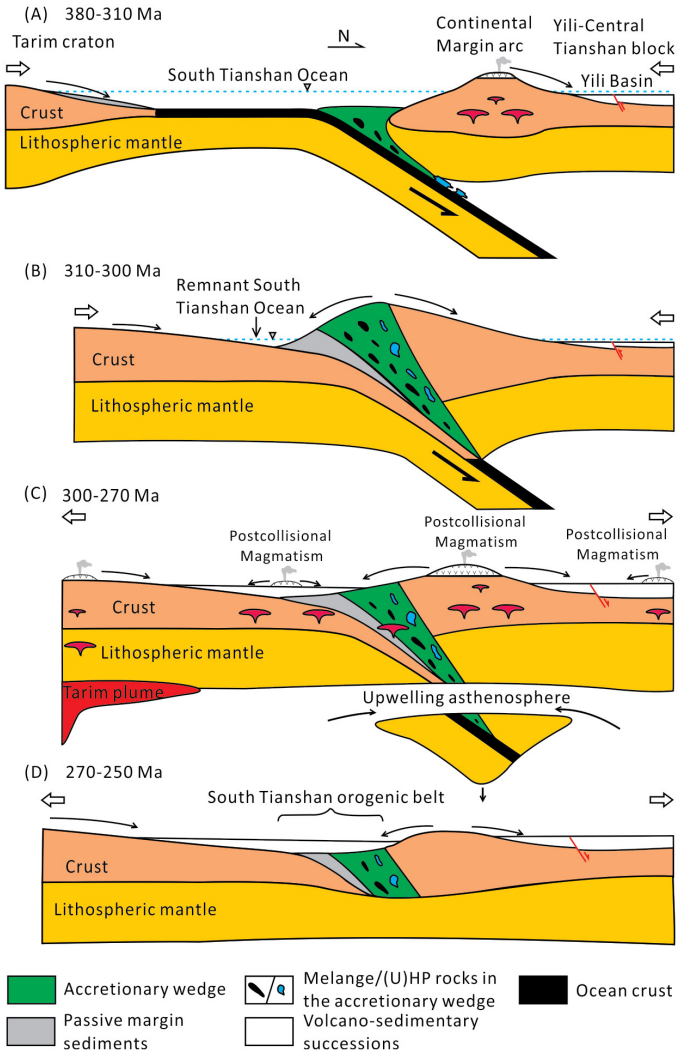

Figure 14. Schematic model illustrating tectonic evolution of the South Tianshan orogen. (U)HP—(ultra)high-pressure.

craton (Fig. 14B). The continent-continent collision and final amalgamation may have resulted in the uplift and erosion of the southern Yili–Central Tianshan block and the (U)HP metamorphic rocks in the northern part of the South Tianshan belt (Fig. 14B). Precambrian zircons in clastic rocks of the Dongtujinhe Formation are rare, indicative of limited basement exposure. The continental deposits at the base of the Dongtujinhe Formation at Tekesi are replaced by shallow-marine deposits. This sedimentary variation is consistent with that in local areas in the South Tianshan belt, where the contemporaneous stratigraphic record shows a change from shallow-marine limestones to deeper-marine, thinly bedded marls interbedded with calcareous sandstones (Alexeiev et al., 2015). These provenance and stratigraphic records suggest that the continent-continent collision may have been discontinuous, consistent with the multiphased deformation in the South Tianshan belt during the late Carboniferous–Early Permian (Alexeiev et al., 2015). Following the strong uplift and erosion in the latest late Carboniferous, the basement in the southern Yili–Central Tianshan block and the (U)HP metamorphic belt in the northern part of the South Tianshan belt were exposed and acted as a source for adjacent detritus.

The Early Permian to earliest Middle Permian clastic rocks from the South Tianshan orogenic and Awulale metallogenic belts show similar detrital zircon age distributions characterized by a near-single age population with peak ages ranging from 299 Ma to 278 Ma (Liu et al., 2013; this study). This single provenance is related to the Early Permian postcollision magmatic rocks in the topographic highland between the southern Yili–Central Tianshan block and the South Tianshan belt (Liu et al., 2013). Early Permian deposition in the South Tianshan belt and southern Yili–Central Tianshan block was controlled by normal faulting and accompanied by bimodal volcanic eruptions (D.D. Liu et al., 2014; D. Li et al., 2015), consistent with a postcollision extensional environment (Han et al., 2011; Gou et al., 2015). During this period (ca. 300–270 Ma), voluminous bimodal volcanic rocks and S-type, A-type, and high-K granites with minor K-rich syenites were extensively developed in the South Tianshan belt, southern Yili–Central Tianshan block, and Awulale metallogenic belt (Fig. 13; D.D. Liu et al., 2014; Chen et al., 2015; Ge et al., 2015; Gou et al., 2015; H. Huang et al., 2015; N.B. Li et al., 2015a; X.X. Ma et al., 2015).

Recently, extensive mafic and felsic igneous rocks with ages of 300–270 Ma have been discovered in the Tarim craton, and they are inferred to form the Tarim large igneous province (Fig. 13; Zhang et al., 2010, 2013; Xu et al., 2014). The South Tianshan belt is situated in the northern Tarim block and may have been affected by the Tarim large igneous province. Nevertheless, on a regional scale, the Permian plutonic rocks in the South Tianshan belt generally extends parallel to the suture (H. Huang et al., 2014, 2015). This linear distribution of plutonic rocks does not favor a plume-related origin (G. Huang et al., 2014, 2015). The significant geodynamic change from convergence to extension in the South Tianshan region may have been related to breakoff of the subducted oceanic slab, accompanied by upwelling of the asthenosphere (Fig. 14C; Han et al., 2011; Ge et al., 2015; Gou et al., 2015; X.X. Ma et al., 2015; Xia et al., 2016). This process may have played an important role in the genesis of the igneous rocks and involved the reworking of ancient crust and mantle-derived sources, consistent with the Hf isotopic compositions (Gou et al., 2015; X.X. Ma et al., 2015). The metamorphic fragments and clasts in the conglomerates and Precambrian zircons in clastic rocks increase from the Middle Permian to Late Permian, with a corresponding decrease in volcanic clasts and late Paleozoic zircons. Importantly, granitic, granitic gneiss, and diabase clasts are present in the Late Permian conglomerates. These provenance trends and petrologic changes suggest a strong planation and erosion of the topographic highland between the southern Yili–Central Tianshan block and South Tianshan belt (Fig. 14D). This is consistent with apatite fission-track analysis and (U-Th)/He dating on apatite and zircon, which showed a major exhumation episode in the southern Yili–Central Tianshan block during the Permian (Jolivet et al., 2010).

CONCLUSIONS

Detrital zircon provenance patterns from the late Paleozoic strata in the Yili Basin indicate derivation of detritus mainly from the southern Yili–Central Tianshan block. Together with (U)HP metamorphic and stratigraphic records, integration of our data from the Yili Basin with data from time-equivalent northern Tarim and South Tianshan regions suggests that the closure of the South Tianshan Ocean, associated with the collision between the Tarim craton and Yili–Central Tianshan block, occurred at ca. 310–300 Ma. Our data support continuous northward subduction of the South Tianshan oceanic crust beneath the Yili–Central Tianshan block from the Late Devonian to late Carboniferous (380–310 Ma). At ca. 310–300 Ma, the continent-continent collision and final amalgamation resulted in the uplift and denudation of the southern Yili–Central Tianshan block and (U)HP metamorphic belt along the northern margin of the South Tianshan orogenic belt. Following collision, the South Tianshan orogenic belt underwent extension associated with the emplacement of large amounts of postcollisional magmatic rocks.

ACKNOWLEDGMENTS

We would like to thank Associate Editor Quentin Crowley and two anonymous reviewers for their constructive comments and suggestions, which substantially improved our manuscript; and Editor Aaron J. Cavosie for editorial handing. We would like to thank Jianghai Yang and Fuhao Xiong for their discussions on the manuscript, and Wenjian Jiang and Xinyi Ge for help during the field work. This research was supported by the 973 Program under grant no. 2015CB453000, the National Natural Science Foundation of China (41502109), the Cultivating Program of Middle-Aged Key Teachers of Chengdu University of Technology (KYGG201718), Innovation Team of Sedimentary Geology of Chengdu University of Technology (KYTD201703), and by the China Postdoctoral Science Foundation (2015M582528). Cawood acknowledges support from the Australian Research Council grant FL160100168.

REFERENCES CITED

Alexeiev, D.V., Ryazantsev, A.V., Kröner, A., Tretyakov, A.A., Xia, X., and Liu, D.Y., 2011, Geochemical data and zircon ages for rocks in a high-pressure belt of Chu-Yili Mountains, southern Kazakhstan: Implications for the earliest stages of accretion in Kazakhstan and the Tianshan: Journal of Asian Earth Sciences, v. 42, p. 805–820, https://doi.org/10.1016/j.jseaes.2010.09.004.

Alexeiev, D.V., Biske, Y.S., Wang, B., Djenchuraeva, A.V., Getman, O.F., Aristov, V.A., Kröner, A., Liu, H., and Zhong, L., 2015, Tectono-stratigraphic framework and Palaeozoic evolution of the Chinese South Tianshan: Geotectonics, v. 49, p. 93–122, https://doi.org/10.1134/S0016852115020028.

An, F., Zhu, Y.F., Wei, S.N., and Lai, S.C., 2013, An Early Devonian to early Carboniferous volcanic arc in North Tianshan, NW China: Geochronological and geochemical evidence from volcanic rocks: Journal of Asian Earth Sciences, v. 78, p. 100–113, https://doi.org/10.1016/j.jseaes.2013.07.037.

An, F., Zhu, Y.F., Wei, S.N., and Lai, S.C., 2017, The zircon U-Pb and Hf isotope constraints on the basement nature and Paleozoic evolution in the northern margin of Yili block, NW China: Gondwana Research, v. 43, p. 41–54, https://doi.org/10.1016/j.gr.2015.11.014.

Bai, J.K., Li, Z.P., Xu, X.Y., Sun, J.M., and Niu, Y.Z., 2015a, Carboniferous volcanic-sedimentary succession and basin properties in Ili area, western Tianshan, Xinjiang: Geological Review, v. 61, p. 195–206 [in Chinese with English abstract].

Bai, J.K., Li, Z.P., Xu, X.Y., and Li, T., 2015b, Tectonic environment of Western Tianshan during the early Carboniferous: Sedimentary and stratigraphical evidence from the bottom of the Dahalajunshan Formation: Acta Sedimentologica Sinica, v. 33, p. 459–469 [in Chinese with English abstract].

Biske, Y.S., and Seltmann, R., 2010, Paleozoic Tian-Shan as a transitional region between the Rheic and Urals-Turkestan oceans: Gondwana Research, v. 17, p. 602–613, https://doi.org/10.1016/j.gr.2009.11.014.

Blair, T.C., and McPherson, J.G., 1994, Alluvial fans and their natural distinction from rivers based on morphology, hydraulic processes, sedimentary processes, and facies assemblages: Journal of Sedimentary Research, v. 64, p. 450–489.

Blichert-Toft, J., and Albarède, F., 1997, The Lu-Hf isotope geochemistry of chondrites and the evolution of the mantle-crust system: Earth and Planetary Science Letters, v. 148, p. 243–258, https://doi.org/10.1016/S0012-821X(97)00040-X.

Carroll, A.R., Dumitru, T.A., Graham, S.A., and Hendrix, M.S., 2013, An 800 million-year detrital zircon record of continental amalgamation: Tarim Basin, NW China: International Geology Review, v. 55, p. 818–829, https://doi.org/10.1080/00206814.2013.787232.

Cawood, P.A., and Nemchin, A.A., 2001, Paleogeographic development of the east Laurentian margin: Constraints from U-Pb dating of detrital zircons in the Newfoundland Appalachians: Geological Society of America Bulletin, v. 113, p. 1234–1246, https://doi.org/10.1130/0016-7606(2001)113<1234:PDOTEL>2.0.CO;2.

Cawood, P.A., Kröner, A., Collins, W.J., Kusky, T.M., Mooney, W.D., and Windley, B.F., 2009, Accretionary orogens through Earth history, *in* Cawood, P.A., and Kröner, A., eds., Earth Accretionary Systems in Space and Time: Geological Society, London, Special Publication 318, p. 1–36, https://doi.org/10.1144/SP318.1.

Cawood, P.A., Hawkesworth, C.J., and Dhuime, B., 2012, Detrital zircon record and tectonic setting: Geology, v. 40, p. 875–878, https://doi.org/10.1130/G32945.1.

Charvet, J., Shu, L.S., Laurent-Charvet, S., Wang, B., Faure, M., Cluzel, D., Chen, Y., and De Jong, K., 2011, Palaeozoic tectonic evolution of the Tianshan belt, NW China: Science China–Earth Sciences, v. 54, p. 166–184, https://doi.org/10.1007/s11430-010-4138-1.

Chen, G.W., Deng, T., Liu, R., Xia, H., and Liu, Q., 2015, Geochemistry of bimodal volcanic rocks in Permian Taerdetao formation in Awulale area of western Tianshan, Xinjiang: Acta Petrologica Sinica, v. 31, p. 105–118 [in Chinese with English abstract].

Cohen, K.M., Finney, S.C., Gibbard, P.L., and Fan, J.X., 2013, The ICS International Chronostratigraphic Chart: Episodes, v. 36, p. 199–204.

De Grave, J., Glorie, S., Buslov, M.M., Izmer, A., Fournier-Carrie, A., Batalev, V.Y., Vanhaecke, F., and Elburg, M., 2011, The thermo-tectonic history of the Song-Kul Plateau, Kyrgyz Tien Shan: Constraints by apatite and titanite thermochronometry and zircon U/Pb dating: Gondwana Research, v. 20, p. 745–763, https://doi.org/10.1016/j.gr.2011.03.011.

Dickinson, W.R., and Gehrels, G.E., 2009, Use of U-Pb ages of detrital zircons to infer maximum depositional ages of strata: A test against a Colorado Plateau Mesozoic database: Earth and Planetary Science Letters, v. 288, p. 115–125, https://doi.org/10.1016/j.epsl.2009.09.013.

Dickinson, W.R., Beard, L.S., Brakenridge, G.R., Erjavec, J.L., Ferguson, R.C., Inman, K.F., Knepp, R.A., Lindberg, F.A., and Ryberg, P.T., 1983, Provenance of North American Phanerozoic sandstones in relation to tectonic setting: Geological Society of America Bulletin, v. 94, p. 222–235, https://doi.org/10.1130/0016-7606(1983)94<222:PONAPS>2.0.CO;2.

Duan, S., Zhang, Z., Jiang, Z., Zhao, J., Zhang, Y., Li, F., and Tian, J., 2014, Geology, geochemistry, and geochronology of the Dunde iron-zinc ore deposit in western Tianshan, China: Ore Geology Reviews, v. 57, p. 441–461, https://doi.org/10.1016/j.oregeorev.2013.08.019.

Gao, J., Long, L.L., Klemd, R., Qian, Q., Liu, D.Y., Xiong, X.M., Su, W., Liu, W., Wang, Y.T., and Yang, F.Q., 2009, Tectonic evolution of the South Tianshan orogen and adjacent regions, NW China: Geochemical and age constraints of granitoid rocks: International Journal of Earth Sciences, v. 98, p. 1221–1238, https://doi.org/10.1007/s00531-008-0370-8.

Gao, J., Klemd, R., Qian, Q., Zhang, X., Li, J., Jiang, T., and Yang, Y.Q., 2011, The collision between the Yili and Tarim blocks of the southwestern Altaids: Geochemical and age constraints of a leucogranite dike crosscutting the HP-LT metamorphic belt in the Chinese Tianshan orogen: Tectonophysics, v. 499, p. 118–131, https://doi.org/10.1016/j.tecto.2011.01.001.

Gao, J., Wang, X.S., Klemd, R., Jiang, T., Qian, Q., Mu, L.X., and Ma, Y.Z., 2015, Record of assembly and breakup of Rodinia in the southwestern Altaids: Evidence from Neoproterozoic magmatism in the Chinese Western Tianshan orogen: Journal of Asian Earth Sciences, v. 113, p. 173–193, https://doi.org/10.1016/j.jseaes.2015.02.002.

Ge, R.F., Zhu, W.B., Wilde, S.A., He, J.W., Cui, X., Wang, X., and Bihai, Z., 2014, Neoproterozoic to Paleozoic long-lived accretionary orogeny in the northern Tarim craton: Tectonics, v. 33, p. 302–329, https://doi.org/10.1002/2013TC003501.

Ge, S.S., Zhai, M.G., Safonova, I., Li, D.P., Zhu, X.Y., Zuo, P.F., and Shan, H.X., 2015, Whole-rock geochemistry and Sr-Nd-Pb isotope systematics of the late Carboniferous volcanic rocks of the Awulale metallogenic belt in the western Tianshan Mountains (NW China): Petrogenesis and geodynamical implications: Lithos, v. 228, p. 62–77, https://doi.org/10.1016/j.lithos.2015.04.019.

Gou, L.L., and Zhang, L.F., 2016, Geochronology and petrogenesis of granitoids and associated mafic enclaves from Xiate in Chinese Southwest Tianshan: Implications for early Paleozoic tectonic evolution: Journal of Asian Earth Sciences, v. 115, p. 40–61, https://doi.org/10.1016/j.jseaes.2015.09.024.

Gou, L.L., Zhang, L.F., Tao, R.B., and Du, J.X., 2012, A geochemical study of syn-subduction and post-collisional granitoids at Muzhaerte River in the Southwest Tianshan UHP belt, NW China: Lithos, v. 136, p. 201–224, https://doi.org/10.1016/j.lithos.2011.10.005.

Gou, L.L., Zhang, L.F., Zeng, L., and Shen, T.T., 2015, Geochemistry and geochronology of S-type granites and their coeval MP/HT metasedimentary rocks in Chinese Southwest Tianshan and their tectonic implications: Journal of Asian Earth Sciences, v. 107, p. 151–171, https://doi.org/10.1016/j.jseaes.2015.04.020.

Griffin, W.L., Pearson, N.J., Belousova, E., Jackson, S.E., Van Achterbergh, E.O., Reilly, S.Y., and Shee, S.R., 2000, The Hf isotope composition of cratonic mantle: LAM-MC-ICPMS analysis of zircon megacrysts in kimberlites: Geochimica et Cosmochimica Acta, v. 64, p. 133–147, https://doi.org/10.1016/S0016-7037(99)00343-9.

Grimes, C.B., Wooden, J.L., Cheadle, M.J., and John, B.E., 2015, "Fingerprinting" tectono-magmatic provenance using trace elements in igneous zircon: Contributions to Mineralogy and Petrology, v. 170, p. 1–26, https://doi.org/10.1007/s00410-015-1199-3.

Han, B.F., Guo, Z.J., Zhang, Z.C., Zhang, L., Chen, J.F., and Song, B., 2010, Age, geochemistry, and tectonic implications of a late Paleozoic stitching pluton in the North Tian Shan suture zone, western China: Geological Society of America Bulletin, v. 122, p. 627–640, https://doi.org/10.1130/B26491.1.

Han, B.F., He, G.Q., Wang, X.C., and Guo, Z., 2011, Late Carboniferous collision between the Tarim and Kazakhstan-Yili terranes in the western segment of the South Tian Shan orogen, Central Asia, and implications for northern Xinjiang, western China: Earth-Science Reviews, v. 109, p. 74–93, https://doi.org/10.1016/j.earscirev.2011.09.001.

Han, Q., Gong, X.P., Ma, H.D., Chen, S.L., Feng, J., Song, X.L., Xie, L., Su, H., and Li, X.L., 2015, Temporal and spatial distribution of Dahalajunshan Group volcanic rocks in the Awulale metallogenic belt of West Tianshan Mountains and its geological significance: Geology in China, v. 42, p. 570–586 [in Chinese with English abstract].

Han, Y.G., Zhao, G.C., Sun, M., Eizenhöfer, P.R., Hou, W.Z., Zhang, X.R., Liu, D.X., Wang, B., and Zhang, G.W., 2015, Paleozoic accretionary orogenesis in the paleo–Asian Ocean: Insights from detrital zircons from Silurian to Carboniferous strata at the northwestern margin of the Tarim craton: Tectonics, v. 34, p. 334–351, https://doi.org/10.1002/2014TC003668.

Han, Y.G., Zhao, G.C., Sun, M., Eizenhöfer, P.R., Hou, W.Z., Zhang, X.R., Liu, Q., Wang, B., Liu, D.X., and Xu, B., 2016a, Late Paleozoic subduction and collision processes during the amalgamation of the Central Asian orogenic belt along the South Tianshan suture zone: Lithos, v. 246–247, p. 1–12, https://doi.org/10.1016/j.lithos.2015.12.016.

Han, Y.G., Zhao, G.C., Cawood, P.A., Sun, M., Eizenhöfer, P.R., Hou, W.Z., Zhang, X.R., and Liu, Q., 2016b, Tarim and North China cratons linked to northern Gondwana through switching accretionary tectonics and collisional orogenesis: Geology, v. 44, p. 95–98, https://doi.org/10.1130/G37399.1.

He, B.Z., Jiao, C.L., Xu, Z.Q., Cai, Z.H., Zhang, J.X., Liu, S.L., Li, H.B., Chen, W.W., and Yu, Z.Y., 2016, The paleotectonic and paleogeography reconstructions of the Tarim Basin and its adjacent areas (NW China) during the late early and middle Paleozoic: Gondwana Research, v. 30, p. 191–206, https://doi.org/10.1016/j.gr.2015.09.011.

Hegner, E., Klemd, R., Kröner, A., Corsini, M., Alexeiev, D.V., Iaccheri, L.M., Zack, T., Dulski, P., Xia, X., and Windley, B.F., 2010, Mineral ages and *P-T* conditions of late Paleozoic high-pressure eclogite and provenance of mélange sediments from Atbashi in the south Tianshan orogen of Kyrgyzstan: American Journal of Science, v. 310, p. 916–950, https://doi.org/10.2475/09.2010.07.

Hu, Z.C., Liu, Y.S., Gao, S., Liu, W.G., Zhang, W., Tong, X.R., Lin, L., Zong, K.Q., Li, M., and Chen, H.H., 2012, Improved in situ Hf isotope ratio analysis of zircon using newly designed X skimmer cone and jet sample cone in combination with the addition of nitrogen by laser ablation multiple collector ICP-MS: Journal of Analytical Atomic Spectrometry, v. 27, p. 1391–1399, https://doi.org/10.1039/c2ja30078h.

Huang, H., Zhang, Z.C., Kusky, T., Santosh, M., Zhang, S., Zhang, D.Y., Liu, J.L., and Zhao, Z.D., 2012a, Continental vertical growth in the transitional zone between South Tianshan and Tarim, western Xinjiang, NW China: Insight from the Permian Halajun A1-type granitic magmatism: Lithos, v. 155, p. 49–66, https://doi.org/10.1016/j.lithos.2012.08.014.

Huang, H., Zhang, Z.C., Kusky, T., Zhang, D.Y., Hou, T., Liu, J.L., and Zhao, Z.D., 2012b, Geochronology and geochemistry of the Chuanwulu complex in the South Tianshan, western Xinjiang, NW China: Implications for petrogenesis and Phanerozoic continental growth: Lithos, v. 140, p. 66–85, https://doi.org/10.1016/j.lithos.2012.01.024.

Huang, H., Zhang, Z.C., Santosh, M., and Zhang, D.Y., 2014, Geochronology, geochemistry and metallogenic implications of the Boziguo'er rare metal–bearing peralkaline granitic intrusion in South Tianshan, NW China: Ore Geology Reviews, v. 61, p. 157–174, https://doi.org/10.1016/j.oregeorev.2014.01.011.

Huang, H., Zhang, Z.C., Santosh, M., Zhang, D.Y., and Wang, T., 2015, Petrogenesis of the Early Permian volcanic rocks in the Chinese South Tianshan: Implications for crustal growth in the Central Asian orogenic belt: Lithos, v. 228, p. 23–42, https://doi.org/10.1016/j.lithos.2015.04.017.

Huang, H., Cawood, P.A., Hou, M.C., Yang, J.H., Ni, S.J., Du, Y.S., Yan, Z.K., and Wang, J., 2016, Silicic ash beds bracket Emeishan large igneous province to < 1 m.y. at ~ 260 Ma: Lithos, v. 264, p. 17–27, https://doi.org/10.1016/j.lithos.2016.08.013.

Huang, Z., Long, X., Kröner, A., Yuan, C., Wang, Y., Chen, B., and Zhang, Y., 2015, Neoproterozoic granitic gneisses in the Chinese Central Tianshan block: Implications for tectonic affinity and Precambrian crustal evolution: Precambrian Research, v. 269, p. 73–89, https://doi.org/10.1016/j.precamres.2015.08.005.

Ingersoll, R.V., Bullard, T.F., Ford, R.L., Grimm, J.P., Pickle, J.D., and Sares, S.W., 1984, The effect of grain size on detrital modes: A test of the Gazzi-Dickinson point-counting method: Journal of Sedimentary Petrology, v. 54, p. 103–116, 10.1306/212F878D-2B24-11D7-8648000102C1865D.

Jackson, S.E., Pearson, N.J., Griffin, W.L., and Belousova, E.A., 2004, The application of laser ablation–inductively coupled plasma–mass spectrometry to in situ U-Pb zircon geochronology: Chemical Geology, v. 211, p. 47–69, https://doi.org/10.1016/j.chemgeo.2004.06.017.

Jian, P., Kröner, A., Jahn, B.M., Liu, D.Y., Zhang, W., Shi, Y.R., and Ma, H.D., 2013, Zircon ages of metamorphic and magmatic rocks within peridotite-bearing mélange: Crucial time constraints on early Carboniferous extensional tectonics in the Chinese Tianshan: Lithos, v. 172, p. 243–266, https://doi.org/10.1016/j.lithos.2013.04.018.

Jiang, T., Gao, J., Klemd, R., Qian, Q., Zhang, X., Xiong, X.M., Wang, X.S., Tan, Z., and Chen, B.X., 2014, Paleozoic ophiolitic mélanges from the South Tianshan Orogen, NW China: Geological, geochemical and geochronological implications for the geodynamic setting: Tectonophysics, v. 612, p. 106–127, https://doi.org/10.1016/j.tecto.2013.11.038.

Jiang, Z.S., Zhang, Z.H., Wang, Z.H., Duan, S.G., Li, F.M., and Tian, J.Q., 2014, Geology, geochemistry, and geochronology of the Zhibo iron deposit in the Western Tianshan, NW China: Constraints on metallogenesis and tectonic setting: Ore Geology Reviews, v. 57, p. 406–424, https://doi.org/10.1016/j.oregeorev.2013.09.016.

Jolivet, M., Dominguez, S., Charreau, J., Chen, Y., Li, Y.G., and Wang, Q.C., 2010, Mesozoic and Cenozoic tectonic history of the central Chinese Tian Shan: Reactivated tectonic structures and active deformation: Tectonics, v. 29, TC6019, https://doi.org/10.1029/2010TC002712.

Jones, J.V., Connelly, J.N., Karlstrom, K.E., Williams, M.L., and Doe, M.F., 2009, Age, provenance, and tectonic setting of Paleoproterozoic quartzite successions in the southwestern United States: Geological Society of America Bulletin, v. 121, p. 247–264, 10.1130/B26351.1.

Klemd, R., Bröcker, M., Hacker, B.R., Gao, J., Gans, P., and Wemmer, K., 2005, New age constraints on the metamorphic evolution of the high-pressure/low-temperature belt in the western Tianshan Mountains, NW China: The Journal of Geology, v. 113, p. 157–168, https://doi.org/10.1086/427666.

Klemd, R., John, T., Scherer, E.E., Rondenay, S., and Gao, J., 2011, Changes in dip of subducted slabs at depth: Petrological and geochronological evidence from HP-UHP rocks (Tianshan, NW-China): Earth and Planetary Science Letters, v. 310, p. 9–20, https://doi.org/10.1016/j.epsl.2011.07.022.

Kröner, A., Alexeiev, D.V., Rojas-Agramonte, Y., Hegner, E., Wong, J., Xia, X., Belousova, E., Mikolaichuk, A.V., Seltmann, R., and Liu, D., 2013, Mesoproterozoic (Grenville-age) terranes in the Kyrgyz North Tianshan: Zircon ages and Nd-Hf isotopic constraints on the origin and evolution of basement blocks in the southern Central Asian orogen: Gondwana Research, v. 23, p. 272–295, https://doi.org/10.1016/j.gr.2012.05.004.

Li, C., Xiao, W.J., Han, C.M., Zhou, K.F., Zhang, J.E., and Zhang, Z.X., 2015, Late Devonian–Early Permian accretionary orogenesis along the North Tianshan in the southern Central Asian orogenic belt: International Geology Review, v. 57, p. 1023–1050, https://doi.org/10.1080/00206814.2014.913268.

Li, D., He, D.F., Tang, Y., Wu, X.Z., Lian, Y.C., and Yang, Y.H., 2015, Dynamic processes from plate subduction to intracontinental deformation: Insights from the tectono-sedimentary evolution of the Zhaosu-Tekesi Depression in the southwestern Chinese Tianshan: Journal of Asian Earth Sciences, v. 113, p. 728–747, https://doi.org/10.1016/j.jseaes.2015.09.007.

Li, J.L., Su, W., Zhang, X., and Liu, X., 2009, Zircon Cameca U-Pb dating and its significance for granulite-facies gneisses from the western Awulale Mountain, West Tianshan, China: Geological Bulletin of China, v. 28, p. 1852–1862 [in Chinese with English abstract].

Li, J.L., Gao, J., and Wang, X.S., 2016, A subduction channel model for exhumation of oceanic-type high-pressure to ultrahigh-pressure eclogite-facies metamorphic rocks in SW Tianshan, China: Science China–Earth Sciences, v. 59, p. 2339–2354, https://doi.org/10.1007/s11430-016-5103-7.

Li, N.B., Niu, H.C., Shan, Q., Jiang, Y.H., Zeng, L.J., Yang, W.B., and Pei, Z.J., 2013, Zircon U-Pb geochronology and geochemistry of post-collisional granitic porphyry from Yuantoushan, Nileke, Xinjiang: Acta Petrologica Sinica, v. 29, p. 3402–3412 [in Chinese with English abstract].

Li, N.B., Niu, H.C., Shan, Q., and Yang, W.B., 2015a, Two episodes of late Paleozoic A-type magmatism in the Qunjisayi area, western Tianshan: Petrogenesis and tectonic implications: Journal of Asian Earth Sciences, v. 113, p. 238–253, https://doi.org/10.1016/j.jseaes.2014.12.015.

Li, N.B., Niu, H.C., Zhang, X.C., Zeng, Q.S., Shan, Q., Li, C.Y., Yan, S., and Yang, W.B., 2015b, Age, petrogenesis and tectonic significance of the ferrobasalts in the Chagangnuoer iron deposit, western Tianshan: International Geology Review, v. 57, p. 1218–1238, https://doi.org/10.1080/00206814.2015.1004136.

Li, Q.L., Lin, W., Su, W., Li, X.H., Shi, Y.H., Liu, Y., and Tang, G.Q., 2011, SIMS U-Pb rutile age of low-temperature eclogites from southwestern Chinese Tianshan, NW China: Lithos, v. 122, p. 76–86, https://doi.org/10.1016/j.lithos.2010.11.007.

Li, T., Xu, X.Y., Li, Z.P., Bai, J.K., and Ru, Y.J., 2012, U-Pb zircon geochronology and geochemistry of the volcanic rocks from Dahalajunshan Formation in Kekesu River area, Western Tianshan Mountains: Geological Bulletin of China, v. 31, p. 1929–1938 [in Chinese with English abstract].

Li, Y.J., Sun, L.D., Wu, H.R., Zhang, G.Y., Wang, G.L., and Huang, Z.B., 2005, Permo-Carboniferous radiolarians from the Wupata'erkan Group, western South Tianshan, Xinjiang, China: Acta Geologica Sinica, v. 79, p. 16–23, https://doi.org/10.1111/j.1755-6724.2005.tb00863.x [in Chinese with English abstract].

Li, Y.J., Yang, G.X., Wang, X.G., Zhang, T.J., Liu, X.Y., Yang, M.Y., and Tong, L.M., 2011, A reconstruction for the late Paleozoic tectonic evolution of the Tekes Daban area, Western Tianshan mountains: Evidence from unconformities: Acta Geologica Sinica [English Edition], v. 85, p. 1127–1136, https://doi.org/10.1111/j.1755-6724.2011.00545.x.

Li, Z., Qiu, N.S., Chang, J., and Yang, X.M., 2015, Precambrian evolution of the Tarim block and its tectonic affinity to other major continental blocks in China: New clues from U-Pb geochronology and Lu-Hf isotopes of detrital zircons: Precambrian Research, v. 270, p. 1–21, https://doi.org/10.1016/j.precamres.2015.09.011.

Liu, C.H., Wu, C.L., Gao, Y.H., Lei, M., Qin, H.P., and Li, M.Z., 2014, Zircon LA-ICP-MS U-Pb dating and Lu-Hf isotopic system of A-type granitoids in South Tianshan, Baicheng County, Xinjiang: Acta Petrologica Sinica, v. 30, p. 1595–1614 [in Chinese with English abstract].

Liu, D.D., Jolivet, M., Yang, W., Zhang, Z.Y., Cheng, F., Zhu, B., and Guo, Z.J., 2013, Latest Paleozoic–early Mesozoic basin-range interactions in South Tian Shan (northwest China) and their tectonic significance: Constraints from detrital zircon U-Pb ages: Tectonophysics, v. 599, p. 197–213, https://doi.org/10.1016/j.tecto.2013.04.018.

Liu, D.D., Guo, Z.J., Jolivet, M., Cheng, F., Song, Y., and Zhang, Z.Y., 2014, Petrology and geochemistry of Early Permian volcanic rocks in South Tian Shan, NW China: Implications for the tectonic evolution and Phanerozoic continental growth: International Journal of Earth Sciences, v. 103, p. 737–756, https://doi.org/10.1007/s00531-013-0994-1.

Liu, H.Q., Xu, Y.G., Tian, W., Zhong, Y.T., Mundil, R., Li, X.H., Yang, Y.H., Luo, Z.Y., and Shang-Guan, S.M., 2014, Origin of two types of rhyolites in the Tarim large igneous province: Consequences of incubation and melting of a mantle plume: Lithos, v. 204, p. 59–72, https://doi.org/10.1016/j.lithos.2014.02.007.

Liu, H.S., Wang, B., Shu, L.S., Jahn, B.M., and Lizuka, Y., 2014, Detrital zircon ages of Proterozoic metasedimentary rocks and Paleozoic sedimentary cover of the northern Yili block: Implications for the tectonics of microcontinents in the Central Asian orogenic belt: Precambrian Research, v. 252, p. 209–222, https://doi.org/10.1016/j.precamres.2014.07.018.

Liu, X., Su, W., Gao, J., Li, J.L., Jiang, T., Zhang, X., and Ge, X.M., 2014, Paleozoic subduction erosion involving accretionary wedge sediments in the South Tianshan orogen: Evidence from geochronological and geochemical studies on eclogites and their host metasediments: Lithos, v. 210, p. 89–110, https://doi.org/10.1016/j.lithos.2014.09.017.

Liu, Y.S., Gao, S., Hu, Z.C., Gao, C.G., Zong, K.Q., and Wang, D.B., 2010, Continental and oceanic crust recycling–induced melt-peridotite interactions in the Trans–North China orogen: U-Pb dating, Hf isotopes and trace elements in zircons from mantle xenoliths: Journal of Petrology, v. 51, p. 537–571, https://doi.org/10.1093/petrology/egp082.

Long, L.L., Gao, J., Wang, J.B., Qian, Q., Xiong, X.M., Wang, Y.W., Wang, L.J., and Gao, L.M., 2008, Geochemistry and SHRIMP zircon U-Pb age of post-collisional granites in the southwest Tianshan orogenic belt of China: Examples from the Heiyingshan and Laohutai plutons: Acta Geologica Sinica [English Edition], v. 82, p. 415–424, 10.1111/j.1755-6724.2008.tb00592.x.

Ludwig, K.R., 2003, User's Manual for Isoplot 3.00: A Geochronological Toolkit for Microsoft Excel: Berkeley Geochronology Center Special Publication 4, 39 p.

Luo, J.H., Che, Z.C., Cao, Y.Z., and Zhang, J.Y., 2008, Geochemical and geochronological characteristics and tectonic significance of Early Permian acid volcanic rocks of Xiaotikanlike Formation in the southern margin of South Tianshan orogen, NW China: Acta Petrologica Sinica, v. 24, p. 2281–2288 [in Chinese with English abstract].

Ma, W.L., Liu, L.F., Song, B., Gao, X.Y., and Deng, S.Z., 2015, Permian sedimentary environment of the west margin of Awulale Mountains, Yili Basin: Journal of China University of Mining & Technology, v. 44, p. 877–884 [in Chinese with English abstract].

Ma, X.X., Shu, L.S., Santosh, M., and Li, J.Y., 2012, Detrital zircon U-Pb geochronology and Hf isotope data from Central Tianshan suggesting a link with the Tarim block: Implications on Proterozoic supercontinent history: Precambrian Research, v. 206, p. 1–16, https://doi.org/10.1016/j.precamres.2012.02.015.

Ma, X.X., Shu, L.S., and Meert, J.G., 2015, Early Permian slab breakoff in the Chinese Tianshan belt inferred from the post-collisional granitoids: Gondwana Research, v. 27, p. 228–243, https://doi.org/10.1016/j.gr.2013.09.018.

Morel, M.L., Nebel, O., Nebel-Jacobsen, Y.J., Miller, J.S., and Vroon, P.Z., 2008, Hafnium isotope characterization of the GJ-1 zircon reference material by solution and laser-ablation MC-ICPMS: Chemical Geology, v. 255, p. 231–235, https://doi.org/10.1016/j.chemgeo.2008.06.040.

Qian, Q., Gao, J., Klemd, R., He, G.Q., Song, B., Liu, D.Y., and Xu, R.H., 2009, Early Paleozoic tectonic evolution of the Chinese South Tianshan orogen: Constraints from SHRIMP zircon U-Pb geochronology and geochemistry of basaltic and dioritic rocks from Xiate, NW China: International Journal of Earth Sciences, v. 98, p. 551–569, https://doi.org/10.1007/s00531-007-0268-x.

Ren, R., Han, B.F., Ji, J.Q., Zhang, L., Xu, Z., and Su, L., 2011, U-Pb age of detrital zircons from the Tekes River, Xinjiang, China, and implications for tectonomagmatic evolution of the South Tian Shan orogen: Gondwana Research, v. 19, p. 460–470, https://doi.org/10.1016/j.gr.2010.07.005.

Scherer, E., Münker, C., and Mezger, K., 2001, Calibration of the lutetium-hafnium clock: Science, v. 293, p. 683–687, https://doi.org/10.1126/science.1061372.

Şengör, A.M.C., Natal'in, B.A., and Burtman, V.S., 1993, Evolution of the Altaid tectonic collage and Palaeozoic crustal growth in Eurasia: Nature, v. 364, p. 299–307, https://doi.org/10.1038/364299a0.

Shu, L.S., Zhu, W.B., Wang, B., Wu, C.Z., Ma, D.S., Ma, X.X., and Ding, H.F., 2013, The formation and evolution of ancient blocks in Xinjiang: Geology in China, v. 40, p. 43–60 [in Chinese with English abstract].

Soldner, J., Oliot, E., Schulmann, K., Štípská, P., Kusbach, V., and Anczkiewicz, R., 2016, Metamorphic *P-T-t-d* evolution of (U)HP metabasites from the South Tianshan accretionary complex (NW China)—Implications for rock deformation during exhumation in a subduction channel: Gondwana Research, v. 47, p. 161–187, https://doi.org/10.1016/j.gr.2016.07.007.

Song, Z.R., Xiao, X.L., Luo, C.L., Wu, M.R., Ling, L.H., and Cheng, C.H., 2005, New advances in the study of Permian stratigraphy at Nileke in the Yinin Basin, Xinjiang: Xinjiang Geology, v. 23, p. 334–338 [in Chinese with English abstract].

Su, W., Gao, J., Klemd, R., Li, J., Zhang, X., Li, X., Chen, N., and Zhang, L., 2010, U-Pb zircon geochronology of Tianshan eclogites in NW China: Implication for the collision between the Yili and Tarim blocks of the southwestern Altaids: European Journal of Mineralogy, v. 22, p. 473–478, https://doi.org/10.1127/0935-1221/2010/0022-2040.

Sun, S.S., and McDonough, W.F., 1989, Chemical and isotopic systematics of oceanic basalts: Implications for mantle composition and processes, *in* Saunders, A.D., and Norry, M.J., Magmatism in the Ocean Basins: Geological Society, London, Special Publication 42, p. 313–345, https://doi.org/10.1144/GSL.SP.1989.042.01.19.

Tang, G.J., Wang, Q., Wyman, D.A., Sun, M., Li, Z.X., Zhao, Z.H., Sun, W.D., Jia, X.H., and Jiang, Z.Q., 2010, Geochronology and geochemistry of late Paleozoic magmatic rocks in the Lamasu-Dabate area, northwestern Tianshan (west China): Evidence for a tectonic transition from arc to post-collisional setting: Lithos, v. 119, p. 393–411, https://doi.org/10.1016/j.lithos.2010.07.010.

Tian, W., Campbell, I.H., Allen, C.M., Guan, P., Pan, W., Chen, M., Yu, H., and Zhu, W., 2010, The Tarim picrite-basalt-rhyolite suite, a Permian flood basalt from northwest China with contrasting rhyolites produced by fractional crystallization and anatexis: Contributions to Mineralogy and Petrology, v. 160, p. 407–425, https://doi.org/10.1007/s00410-009-0485-3.

Tucker, R.T., Roberts, E.M., Hu, Y., Kemp, A.I., and Salisbury, S.W., 2013, Detrital zircon age constraints for the Winton Formation, Queensland: Contextualizing Australia's Late Cretaceous dinosaur faunas: Gondwana Research, v. 24, p. 767–779, https://doi.org/10.1016/j.gr.2012.12.009.

Vervoort, J.D., and Blichert-Toft, J., 1999, Evolution of the depleted mantle: Hf isotope evidence from juvenile rocks through time: Geochimica et Cosmochimica Acta, v. 63, p. 533–556, https://doi.org/10.1016/S0016-7037(98)00274-9.

Wang, B., Shu, L.S., Cluzel, D., Faure, M., and Charvet, J., 2007, Geochemical constraints on Carboniferous volcanic rocks of the Yili block (Xinjiang, NW China): Implication for the tectonic evolution of Western Tianshan: Journal of Asian Earth Sciences, v. 29, p. 148–159, https://doi.org/10.1016/j.jseaes.2006.02.008.

Wang, B., Cluzel, D., Shu, L.S., Faure, M., Charvet, J., Chen, Y., Meffre, S., and De Jong, K., 2009, Evolution of calc-alkaline to alkaline magmatism through Carboniferous convergence to Permian transcurrent tectonics, western Chinese Tianshan: International Journal of Earth Sciences, v. 98, p. 1275–1298, https://doi.org/10.1007/s00531-008-0408-y.

Wang, B., Faure, M., Shu, L., de Jong, K., Charvet, J., Cluzel, D., Jahn, B.M., Chen, Y., and Ruffet, G., 2010, Structural and geochronological study of high-pressure metamorphic rocks in the Kekesu section (northwestern China): Implications for the late Paleozoic tectonics of the Southern Tianshan: The Journal of Geology, v. 118, p. 59–77, https://doi.org/10.1086/648531.

Wang, B., Shu, L.S., Faure, M., Jahn, B.M., Cluzel, D., Charvet, J., Chung, S.L., and Meffre, S.B., 2011, Paleozoic tectonics of the southern Chinese Tianshan: Insights from structural, chronological and geochemical studies of the Heiyingshan ophiolitic mélange (NW China): Tectonophysics, v. 497, p. 85–104, https://doi.org/10.1016/j.tecto.2010.11.004.

Wang, B., Liu, H.S., Shu, L.S., Jahn, B.M., Chung, S.L., Zhai, Y.Z., and Liu, D.Y., 2014a, Early Neoproterozoic crustal evolution in northern Yili block: Insights from migmatite, orthogneiss and leucogranite of the Wenquan metamorphic complex in the NW Chinese Tianshan: Precambrian Research, v. 242, p. 58–81, https://doi.org/10.1016/j.precamres.2013.12.006.

Wang, B., Shu, L.S., Liu, H.S., Gong, H.J., Ma, Y.Z., Mu, L.X., and Zhong, L.L., 2014b, First evidence for ca. 780Ma intra-plate magmatism and its implications for Neoproterozoic rifting of the North Yili block and tectonic origin of the continental blocks in SW of Central Asia: Precambrian Research, v. 254, p. 258–272, https://doi.org/10.1016/j.precamres.2014.09.005.

Wang, H.L., Xu, X.Y., He, H.P., and Chen, J.L., 2007, Geological Map of the Chinese Tian Shan and its Adjacent Areas: Beijing, Geological Publishing House, scale 1:1,000,000, 2 sheets.

Wang, M., Zhang, J.J., Qi, G.W., and Liu, J., 2014, Geochemistry and geochronology of Early Permian acid volcanic rocks along Kuqa River and its tectonic implication in the southern margin of South Tianshan orogen, Xinjiang: Chinese Journal of Geology, v. 49, p. 242–258 [in Chinese with English abstract].

Wiedenbeck, M., Alle, P., Corfu, F., Griffin,W.L., Meier, M., Oberli, F., Quadt, A., Roddick, J.C., and Spiegel, W., 1995, Three natural zircon standards for U-Th-Pb, Lu-Hf, trace element and REE analyses: Geostandards and Geoanalytical Research, v. 19, p. 1–23, https://doi.org/10.1111/j.1751-908X.1995.tb00147.x.

Wilhem, C., Windley, B.F., and Stampfli, G.R.M., 2012, The Altaids of Central Asia: A tectonic and evolutionary innovative review: Earth-Science Reviews, v. 113, p. 303–341, https://doi.org/10.1016/j.earscirev.2012.04.001.

Windley, B.F., Alexeiev, D., Xiao, W.J., Kröner, A., and Badarch, G., 2007, Tectonic models for accretion of the Central Asian orogenic belt: Journal of the Geological Society [of London], v. 164, p. 31–47, https://doi.org/10.1144/0016-76492006-022.

Wu, F.Y., Ji, W.Q., Liu, C.Z., and Chung, S.L., 2010, Detrital zircon U-Pb and Hf isotopic data from the Xigaze fore-arc basin: Constraints on Transhimalayan magmatic evolution in southern Tibet: Chemical Geology, v. 271, p. 13–25, https://doi.org/10.1016/j.chemgeo.2009.12.007.

Wu, F.Y., Ji, W.Q., Wang, J.G., Liu, C.Z., Chung, S.L., and Clift, P.D., 2014, Zircon U-Pb and Hf isotopic constraints on the onset time of India-Asia collision: American Journal of Science, v. 314, p. 548–579, https://doi.org/10.2475/02.2014.04.

Wu, H.R., and Li, Z., 2013, Palaeogeographic and tectonic evolution of South Tianshan Ocean: Re-examination of radiolarian cherts and stratigraphic record of southwestern Tianshan: Journal of Palaeogeography, v. 15, p. 293–304 [in Chinese with English abstract].

Xia, B., Zhang, L.F., Xia, Y., and Bader, T., 2014, The tectonic evolution of the Tianshan orogenic belt: Evidence from U-Pb dating of detrital zircons from the Chinese southwestern Tianshan accretionary mélange: Gondwana Research, v. 25, p. 1627–1643, https://doi.org/10.1016/j.gr.2013.06.015.

Xia, B., Zhang, L.F., Bader, T., Shen, T.T., and Chen, N.S., 2016, Late Palaeozoic $^{40}Ar/^{39}Ar$ ages of the HP-LT metamorphic rocks from the Kekesu Valley, Chinese southwestern Tianshan: New constraints on exhumation tectonics: International Geology Review, v. 58, p. 389–404, https://doi.org/10.1080/00206814.2015.1084487.

Xia, L.Q., Xu, X., Xia, Z.C., Li, X.M., Ma, Z.P., and Wang, L.S., 2004, Petrogenesis of Carboniferous rift-related volcanic rocks in the Tianshan, northwestern China: Geological Society of America Bulletin, v. 116, p. 419–433, https://doi.org/10.1130/B25243.1.

Xia, L.Q., Xia, Z.C., Xu, X.Y., Li, X.M., and Ma, Z.P., 2008, Relative contributions of crust and mantle to the generation of the Tianshan Carboniferous rift-related basic lavas, northwestern China: Journal of Asian Earth Sciences, v. 31, p. 357–378, https://doi.org/10.1016/j.jseaes.2007.07.002.

Xia, L.Q., Xu, X.Y., Li, X.M., Ma, Z.P., and Xia, Z.C., 2012, Reassessment of petrogenesis of Carboniferous–Early Permian rift-related volcanic rocks in the Chinese Tianshan and its neighboring areas: Geoscience Frontiers, v. 3, p. 445–471, https://doi.org/10.1016/j.gsf.2011.12.011.

Xiao, W.J., Windley, B.F., Huang, B.C., Han, C.M., Yuan, C., Chen, H.L., Sun, M., Sun, S., and Li, J.L., 2009, End-Permian to mid-Triassic termination of the accretionary processes of the southern Altaids: Implications for the geodynamic evolution, Phanerozoic continental growth, and metallogeny of Central Asia: International Journal of Earth Sciences, v. 98, p. 1189–1217, https://doi.org/10.1007/s00531-009-0419-3.

Xiao, W.J., Windley, B.F., Allen, M.B., and Han, C.M., 2013, Paleozoic multiple accretionary and collisional tectonics of the Chinese Tianshan orogenic collage: Gondwana Research, v. 23, p. 1316–1341, https://doi.org/10.1016/j.gr.2012.01.012.

Xiao, W.J., Windley, B., Sun, S., Li, J.L., Huang, B.C., Han, C.M., Yuan, C., Sun, M., and Chen, H.L., 2015, A tale of amalgamation of three collage systems in the Permian–Middle Triassic in Central-East Asia: Oroclines, sutures, and terminal accretion: Annual Review of Earth and Planetary Sciences, v. 43, p. 477–507, https://doi.org/10.1146/annurev-earth-060614-105254.

Xiong, S.Y., Yu, C.F., Li, Y.W., and Huang, L., 2011, Sedimentary characteristics and evolution of the Lower Carboniferous Akeshake Formation in the Yili Basin: Acta Petrolei Sinica, v. 32, p. 797–805 [in Chinese with English abstract].

Xu, X.Y., Xia, L.Q., Ma, Z.P., Wang, Y.B., Xia, Z.C., Li, X.M., and Wang, L.S., 2006, SHRIMP zircon U-Pb geochronology of the plagiogranites from Bayringou ophiolite in North Tianshan Mountains and the petrogenesis of the ophiolite: Acta Petrologica Sinica, v. 22, p. 83–94 [in Chinese with English abstract].

Xu, X.Y., Wang, H.L., Li, P., Chen, J., Ma, Z.P., Zhu, T., Wang, N., and Dong, Y.P., 2013, Geochemistry and geochronology of Paleozoic intrusions in the Nalati (Narati) area in western Tianshan, Xinjiang, China: Implications for Paleozoic tectonic evolution: Journal of Asian Earth Sciences, v. 72, p. 33–62, https://doi.org/10.1016/j.jseaes.2012.11.023.

Xu, Y.G., Wei, X., Luo, Z.Y., Liu, H.Q., and Cao, J., 2014, The Early Permian Tarim large igneous province: Main characteristics and a plume incubation model: Lithos, v. 204, p. 20–35, https://doi.org/10.1016/j.lithos.2014.02.015.

Xu, Z.Q., He, B.Z., Zhang, C.L., Zhang, J.X., Wang, Z., and Cai, Z.H., 2013, Tectonic framework and crustal evolution of the Precambrian basement of the Tarim block in NW China: New geochronological evidence from deep drilling samples: Precambrian Research, v. 235, p. 150–162, https://doi.org/10.1016/j.precamres.2013.06.001.

Yan, S., Shan, Q., Niu, H.C., Yang, W.B., Li, N.B., Zeng, L.J., and Jiang, Y.H., 2015, Petrology and geochemistry of late Carboniferous hornblende gabbro from the Awulale Mountains, western Tianshan (NW China): Implication for an arc–nascent back-arc environment: Journal of Asian Earth Sciences, v. 113, p. 218–237, https://doi.org/10.1016/j.jseaes.2015.01.016.

Yang, J.H., Cawood, P.A., Du, Y.S., Huang, H., Huang, H.W., and Tao, P., 2012, Large igneous province and magmatic arc sourced Permian-Triassic volcanogenic sediments in China: Sedimentary Geology, v. 261–262, p. 120–131, https://doi.org/10.1016/j.sedgeo.2012.03.018.

Yang, J.H., Cawood, P.A., and Du, Y.S., 2015, Voluminous silicic eruptions during Late Permian Emeishan igneous province and link to climate cooling: Earth and Planetary Science Letters, v. 432, p. 166–175, https://doi.org/10.1016/j.epsl.2015.09.050.

Yang, J.S., Xu, X.Z., Li, T.F., Chen, S.Y., Ren, Y.F., Li, J.Y., and Liu, Z., 2011, U-Pb ages of zircons from ophiolite and related rocks in the Kumishi region at the southern margin of Middle Tianshan, Xinjiang: Evidence of early Paleozoic oceanic basin: Acta Petrologica Sinica, v. 27, p. 77–95 [in Chinese with English abstract].

Yang, W., Jolivet, M., Dupont Nivet, G., Guo, Z., Zhang, Z., and Wu, C., 2013, Source to sink relations between the Tian Shan and Junggar Basin (northwest China) from late Palaeozoic to Quaternary: Evidence from detrital U-Pb zircon geochronology: Basin Research, v. 25, p. 219–240, https://doi.org/10.1111/j.1365-2117.2012.00558.x.

Yang, W.B., Niu, H.C., Shan, Q., Luo, Y., Sun, W.D., Li, C.Y., Li, N.B., and Yu, X.Y., 2012, Late Paleozoic calc-alkaline to shoshonitic magmatism and its geodynamic implications, Yuximolegai area, western Tianshan, Xinjiang: Gondwana Research, v. 22, p. 325–340, https://doi.org/10.1016/j.gr.2011.10.008.

Yang, X., Zhang, L.F., Tian, Z.L., and Bader, T., 2013, Petrology and U-Pb zircon dating of coesite-bearing metapelite from the Kebuerte Valley, western Tianshan, China: Journal of Asian Earth Sciences, v. 70, p. 295–307, https://doi.org/10.1016/j.jseaes.2013.03.020.

Yu, X.Q., Wang, Z.X., Zhou, X., Xiao, W.F., and Yang, X.P., 2016, Zircon U-Pb geochronology and Sr-Nd isotopes of volcanic rocks from the Dahalajunshan Formation: Implications for Late Devonian–middle Carboniferous tectonic evolution of the Chinese Western Tianshan: International Journal of Earth Sciences, v. 105, no. 5, p. 1637–1661, https://doi.org/10.1007/s00531-015-1275-y.

Zhang, C.L., and Zou, H.B., 2013, Permian A-type granites in Tarim and western part of Central Asian orogenic belt (CAOB): Genetically related to a common Permian mantle plume?: Lithos, v. 172, p. 47–60, https://doi.org/10.1016/j.lithos.2013.04.001.

Zhang, C.L., Li, X.H., Li, Z.X., Ye, H.M., and Li, C.N., 2008, A Permian layered intrusive complex in the Western Tarim block, Northwestern China: Product of a ca. 275-Ma mantle plume?: The Journal of Geology, v. 116, p. 269–287, https://doi.org/10.1086/587726 [in Chinese with English abstract].

Zhang, C.L., Xu, Y.G., Li, Z.X., Wang, H.Y., and Ye, H.M., 2010, Diverse Permian magmatism in the Tarim block, NW China: Genetically linked to the Permian Tarim mantle plume?: Lithos, v. 119, p. 537–552, https://doi.org/10.1016/j.lithos.2010.08.007.

Zhang, D.Y., Zhang, Z.C., Santosh, M., Cheng, Z.G., He, H., and Kang, J.L., 2013, Perovskite and baddeleyite from kimberlitic intrusions in the Tarim large igneous province signal the onset of an end-Carboniferous mantle plume: Earth and Planetary Science Letters, v. 361, p. 238–248, https://doi.org/10.1016/j.epsl.2012.10.034.

Zhang, L.F., Ai, Y.L., Li, X.P., Rubatto, D., Song, B., Williams, S., Song, S.G., Ellis, D., and Liou, J.G., 2007, Triassic collision of western Tianshan orogenic belt, China: Evidence from SHRIMP U-Pb dating of zircon from HP/UHP eclogitic rocks: Lithos, v. 96, p. 266–280, https://doi.org/10.1016/j.lithos.2006.09.012.

Zhang, T.J., Li, Y.J., Wang, X.G., Luan, X.D., Wang, Y.P., Liu, J., Li, H., and Yang, G.X., 2006, Fossil evidence for the Dongtujinhe Formation of Yishenjilike Mountain, Western Tianshan: Xinjiang Geology, v. 24, p. 13–15 [in Chinese with English abstract].

Zhang, X., Klemd, R., Gao, J., Dong, L.H., Wang, X.S., Haase, K., Jiang, T., and Qian, Q., 2015, Metallogenesis of the Zhibo and Chagangnuoer volcanic iron oxide deposits in the Awulale iron metallogenic belt, Western Tianshan orogen, China: Journal of Asian Earth Sciences, v. 113, p. 151–172, https://doi.org/10.1016/j.jseaes.2014.06.004.

Zhang, X., Tian, J.Q., Gao, J., Klemd, R.N., Dong, L.H., Fan, J.J., Jiang, T., Hu, C.J., and Qian, Q., 2012, Geochronology and geochemistry of granitoid rocks from the Zhibo syngenetic volcanogenic iron ore deposit in the Western Tianshan Mountains (NW-China): Constraints on the age of mineralization and tectonic setting: Gondwana Research, v. 22, p. 585–596, https://doi.org/10.1016/j.gr.2011.06.007.

Zhang, X.R., Zhao, G.C., Sun, M., Eizenhöfer, P.R., Han, Y.G., Hou, W.Z., Liu, D.X., Wang, B., Liu, Q., and Xu, B., 2016, Tectonic evolution from subduction to arc-continent collision of the Junggar ocean: Constraints from U-Pb dating and Hf isotopes of detrital zircons from the North Tianshan belt, NW China: Geological Society of America Bulletin, v. 128, p. 644–660, https://doi.org/10.1130/B31230.1.

Zhao, X.B., Xue, C.J., Symons, D.T., Zhang, Z.C., and Wang, H.G., 2014, Microgranular enclaves in island-arc andesites: A possible link between known epithermal Au and potential porphyry Cu-Au deposits in the Tulasu ore cluster, western Tianshan, Xinjiang, China: Journal of Asian Earth Sciences, v. 85, p. 210–223, https://doi.org/10.1016/j.jseaes.2014.01.014.

Zhao, Z.Y., Zhang, Z.C., Santosh, M., Huang, H., Cheng, Z.G., and Ye, J.C., 2015, Early Paleozoic magmatic record from the northern margin of the Tarim craton: Further insights on the evolution of the Central Asian orogenic belt: Gondwana Research, v. 28, p. 328–347, https://doi.org/10.1016/j.gr.2014.04.007.

Zhu, Y., Zhang, L., Gu, L., Guo, X., and Zhou, J., 2005, The zircon SHRIMP chronology and trace element geochemistry of the Carboniferous volcanic rocks in western Tianshan Mountains: Chinese Science Bulletin, v. 50, p. 2201–2212, https://doi.org/10.1007/BF03182672.

Zhu, Y.F., 2012, The zircon U-Pb age for the Neoproterozoic–Ordovician granites in the Kesang Rongdong region, southwestern Tianshan Mts., Xinjiang: Acta Petrologica Sinica, v. 28, p. 2113–2120 [in Chinese with English abstract].

Zhu, Y.F., Guo, X., Song, B., Zhang, L.F., and Gu, L.B., 2009, Petrology, Sr-Nd-Hf isotopic geochemistry and zircon chronology of the Late Palaeozoic volcanic rocks in the southwestern Tianshan Mountains, Xinjiang, NW China: Journal of the Geological Society [of London], v. 166, p. 1085–1099, https://doi.org/10.1144/0016-76492008-130.

Zhu, Y.F., An, F., Xue, Y.X., Chen, B., and Zhang, L.F., 2010, Zircon U-Pb age for Kesang Rondong volcanic rocks, Southwest Tianshan Mts., Tekes, Xinjiang: Acta Petrologica Sinica, v. 26, p. 2255–2263 [in Chinese with English abstract].

Zhu, Z.X., Wang, K.Z., Zheng, Y.J., Sun, G.H., Zhang, C., and Li, Y.P., 2006, Zircon SHRIMP dating of Silurian and Devonian granitic intrusions in the southern Yili block, Xinjiang, and preliminary discussion on their tectonic setting: Acta Petrologica Sinica, v. 22, p. 1193–1200 [in Chinese with English abstract].

Zou, S.Y., Li, Z.L., Ren, Z.Y., Li, Y.Q., Yang, S.F., Chen, H.L., Song, B., and Yu, X., 2013, U-Pb dating and Hf isotopic compositions of detrital zircons from Permian sedimentary rocks in Keping area of Tarim Basin, Xinjiang, China: Constraints on geological evolution of Tarim block: Acta Petrologica Sinica, v. 29, p. 3369–3388 [in Chinese with English abstract].

Science Editor: Aaron J. Cavosie
Associate Editor: Quentin G. Crowley

Manuscript Received 3 June 2016
Revised Manuscript Received 28 August 2017
Manuscript Accepted 1 November 2017

Printed in the USA